



Methane flux from Beringian coastal wetlands for the past 20,000 years



Matthias Fuchs ^{a,b,*}, Miriam C. Jones ^c, Evan J. Gowan ^{d,e}, Steve Frolking ^f,
Katey Walter Anthony ^g, Guido Grosse ^{b,h}, Benjamin M. Jones ⁱ, Jonathan A. O'Donnell ^j,
Laura Brosius ^g, Claire Treat ^b

^a Renewable and Sustainable Energy Institute, University of Colorado Boulder, 4001 Discovery Drive, Boulder, CO 80303, USA

^b Alfred Wegener Institute Helmholtz Centre for Polar and Marine Research, Permafrost Research Section, Telegrafenberg A45, 14473, Potsdam, Germany

^c US Geological Survey, Florence Bascom Geoscience Center, 12201 Sunrise Valley Dr, Reston, VA 20192, USA

^d Department of Earth and Environmental Sciences, Kumamoto University, 2-39-1 Kurokami, Chuoku, 860-8555, Kumamoto, Japan

^e KIKAI Institute for Coral Reef Sciences, Kagoshima, Japan

^f Institute for the Study of Earth, Oceans, and Space, University of New Hampshire, Durham, NH, 03824, USA

^g Water and Environmental Research Center, Institute of Northern Engineering, University of Alaska Fairbanks, PO Box 755910, Fairbanks, AK, 99775, USA

^h University of Potsdam, Institute of Geosciences, 14476 Potsdam, Germany

ⁱ Institute of Northern Engineering, University of Alaska Fairbanks, PO Box 755910, Fairbanks, AK, 99775, USA

^j Arctic Network, National Park Service, 240 W 5th Avenue, Anchorage, AK 99501, USA

ARTICLE INFO

Handling Editor: I Hendy

Original content: <https://doi.org/10.1594/PANGAEA.960150>
<https://doi.org/10.1594/PANGAEA.960160>
<https://doi.org/10.1594/PANGAEA.960156>

Keywords:

Methane
Beringia
Sea-level rise
Arctic
Paleo reconstruction

ABSTRACT

Atmospheric methane (CH_4) concentrations have gone through rapid changes since the last deglaciation; however, the reasons for abrupt increases around 14,700 and 11,600 years before present (yrs BP) are not fully understood. Concurrent with deglaciation, sea-level rise gradually inundated vast areas of the low-lying Beringian shelf. This transformation of what was once a terrestrial-permafrost tundra-steppe landscape, into coastal, and subsequently, marine environments led to new sources of CH_4 from the region to the atmosphere. Here, we estimate, based on an extended geospatial analysis, the area of Beringian coastal wetlands in 1000-year intervals and their potential contribution to northern CH_4 flux (based on present day CH_4 fluxes from coastal wetland) during the past 20,000 years. At its maximum (\sim 14,000 yrs BP) we estimated CH_4 fluxes from Beringia coastal wetlands to be 3.5 ($+4.0/-1.9$) Tg CH_4 yr $^{-1}$. This shifts the onset of CH_4 fluxes from northern regions earlier, towards the Bølling-Allerød, preceding peak emissions from the formation of northern high latitude thermokarst lakes and wetlands. Emissions associated with the inundation of Beringian coastal wetlands better align with polar ice core reconstructions of northern hemisphere sources of atmospheric CH_4 during the last deglaciation, suggesting a connection between rising sea level, coastal wetland expansion, and enhanced CH_4 emissions.

1. Introduction

Atmospheric greenhouse gas concentrations underwent major changes in the past 20,000 years (Marcott et al., 2014; Severinghaus and Brook, 1999). Based on ice core data (Brook et al., 1996; Köhler et al., 2017), an abrupt, near doubling of atmospheric methane (CH_4) in a timescale of decades to centuries occurred at 14,700 years before present (yrs BP) and 11,600 yrs BP. However, the origins of these sudden atmospheric CH_4 concentration rises are so far not fully understood. While tropical wetlands likely played a role in the rise of the deglacial atmospheric CH_4 concentration in the Northern Hemisphere (Bock et al., 2017), northern (extratropical) latitudes (30 – 90°N) are estimated to

have contributed up to 71 Tg CH_4 yr $^{-1}$ during 11,500–9500 yrs BP (Brook et al., 2000; Yang et al., 2017). Although northern high latitude peatlands (Treat et al., 2021) and lakes (Brosius et al., 2012, 2023) became significant CH_4 sources at the onset of the Holocene, they cannot fully explain the increase in atmospheric CH_4 concentrations during early Deglaciation. Therefore, the reasons for these steep CH_4 increases at 14,700 yrs BP remain unresolved. Furthermore, ^{14}C - CH_4 analyses of the polar ice cores suggest that the source of northern high latitude atmospheric CH_4 concentration reflected a microbial origin based on contemporary carbon, which indicates wetlands as a main driver for the rise of atmospheric CH_4 concentrations (Dyonisius et al., 2020; Petrenko et al., 2017).

* Corresponding author. Renewable and Sustainable Energy Institute, University of Colorado Boulder, 4001 Discovery Drive, Boulder, CO 80303, USA.
 E-mail address: matthias.fuchs@colorado.edu (M. Fuchs).

During the past 20,000 years, more than $2.8 \times 10^6 \text{ km}^2$ of previously unglaciated coastal, near-shore areas of today's Bering, Chukchi, Laptev, and East Siberian seas were flooded due to the melting of the Laurentide, Cordilleran, and Eurasian ice sheets. This now-inundated shelf and land area (an area larger than Greenland), is known as 'Beringia' (Fig. 1) and was largely unglaciated during the Last Glacial Maximum (Hopkins, 1967; Schirrmeyer et al., 2013; Sher, 1991). Within this unglaciated region, carbon-cycle processes in coastal regions, particularly CH_4 fluxes, are largely unconstrained in the paleo record.

Low-lying coastal areas are prone to flooding due to sea-level rise, and expansion of coastal wetlands might enhance the C stored in coastal deposits (Mcleod et al., 2011; Rogers et al., 2019). However, with increased flooding, newly inundated coastal areas can become CH_4 emitting wetlands. While CH_4 emissions from tidal wetlands in general decrease with increasing salinity, there is still large variability in the available CH_4 flux data from tidal wetlands (Poffenbarger et al., 2011). Tidal wetlands, which can have high salinity variability, can be important CH_4 sources, partly offsetting C sequestration (Rosentreter et al., 2018). Currently, coastal wetlands and tidal flats are estimated to have a mean CH_4 flux into the atmosphere of $14.6 \text{ Tg CH}_4 \text{ yr}^{-1}$ (Rosentreter et al., 2021a), but a changing climate (higher temperatures, elevated CO_2 levels, eutrophication) with increasing sea-level can lead to different magnitudes of CH_4 emissions from tidal wetlands (Mueller et al., 2020; Rosentreter et al., 2021b).

The low relief of Beringia suggests sea-level inundation during deglaciation could have substantially increased coastal wetland area and contributed to the rise in atmospheric CH_4 concentrations, but neither

the size of these wetlands nor magnitude of potential CH_4 release have yet been quantified. This study aims to address the question to what degree Beringian coastal wetlands contributed to the rise in atmospheric CH_4 concentration over the last deglacial/sea-level transgression in the Northern Hemisphere. In consequence, we estimate the size and timing of coastal wetland development for the past 20,000 years and upscale the potential CH_4 fluxes from these areas based on present-day CH_4 flux analogs.

2. Regional setting

Beringia spans the region between northeastern Siberia and eastern Alaska, which includes the continental shelf that was exposed during the Last Glacial Maximum (LGM) lowstand that now comprises the Bering, Chukchi, Laptev/East Siberian Seas and the shelf of the Beaufort Sea (Fig. 1). For this study, we focus on the continental shelf, which has been flooded during the past 20,000 years. This shelf domain spans more than $2,800,000 \text{ km}^2$ with areas up to 100 m below current sea-level, and with an average depth of 39 m. This continental shelf domain extends up to 800 km northwards of the present-day Arctic coastline and has a mean slope of 0.03° , highlighting the flat, low relief of the vast Beringian shelf (Jakobsson et al., 2020).

The flooding of the Beringian shelf (Fig. 2) at the end of the LGM was a result of the retreating ice sheets. In the initial phase (20,000–10,000 yrs BP), sea-level rose rapidly until mid to late Holocene (Supplementary Material Fig. S1) (Pico et al., 2020) until the land connection between Siberia and Alaska became flooded. Estimates for the complete flooding

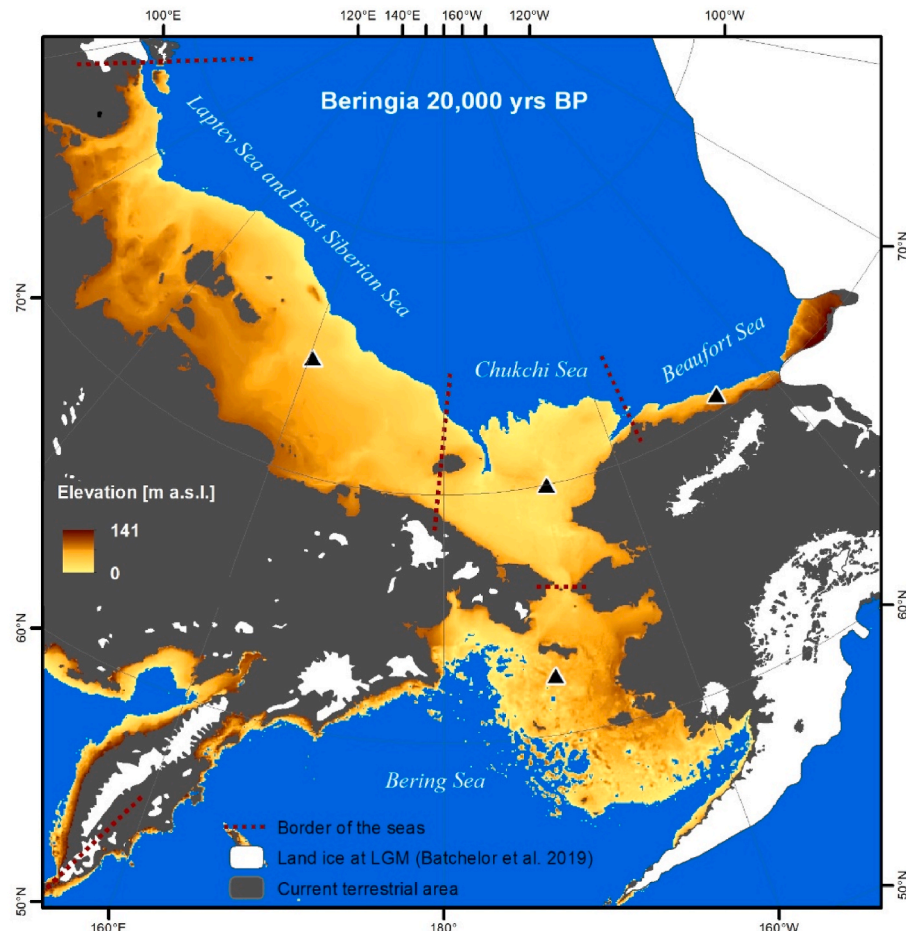


Fig. 1. The landmass of Beringia at 20,000 yrs BP (elevation above low-stand sea level in yellow-brownish colors). Red dotted lines indicate the borders of the different seas for the spatial flooding estimation (see results section). Black triangles indicate points where the relative sea level data (Fig. S1) were extracted from the Gowan et al. (2021) data set; ice sheet data from Batchelor et al. (2019).

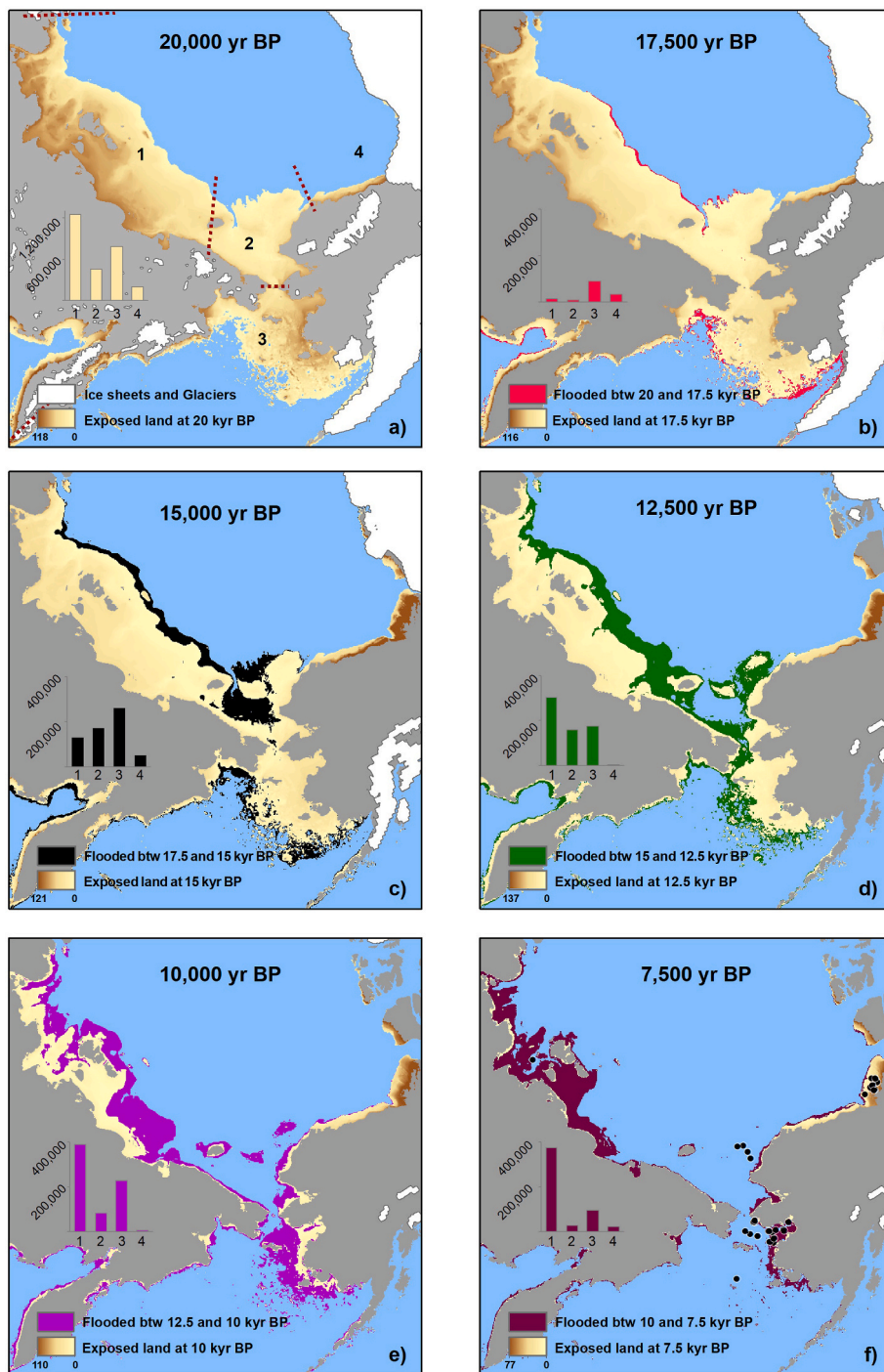


Fig. 2. Flooding of Beringia for different time periods. Timing of flooding in Beringia is based on PaleoMIST 1.0 (Gowan et al., 2021). Panel a) shows the extent of Beringia at 20,000 yrs BP with the borders of the different regions (dashed lines) and the ice sheets in Alaska and Canada (Gowan et al., 2021) and Siberia (Batchelor et al., 2019), and the total area of each region in km² (graph); 1: Laptev and East Siberian seas, 2: Chukchi Sea, 3: Bering Sea, 4: Beaufort Sea. Areas are derived from analysis of paleo bathymetry grids from Gowan et al. (2021). Panels b) – f) show the exposed land area in meters above sea-level (in gold colors) of Beringia (see also Fig. S1c for the behavior of sea level development for the different regions). Ice sheets (white) for Alaska are based on Gowan et al. (2021) for the time b) 17,500 yrs BP, c) 15,000 yrs BP, d) 12,500 yrs BP, e) 10,000 yrs BP, and f) 7500 yrs BP. Panel f) includes the location of ¹⁴C samples (black dots) used to validate the model (see Fig. 3). The graphs in panels b) – f) show the newly flooded area for each region in km². Contemporary land area (0 yrs BP) is grey.

of the Bering Land Bridge range between 13,000 yrs BP and 10,500 yrs BP and are based on different paleo proxies such as molluscs (England and Furze, 2008), remains of a Bowhead whale (Dyke et al., 2011), buried peat (Elias et al., 1992, 1996), and benthic foraminifera (Keigwin et al., 2006). Jakobsson et al. (2017) concluded that the Bering Land Bridge was flooded at around 11,000 yrs BP based on a dated core from the Herald Canyon in the Chukchi Sea.

The flooding of the Bering Land Bridge had major biogeographical and climatic implications, but rising sea-level and changing climate in Beringia also fundamentally altered the biogeochemistry and carbon cycling of the landscape. The vast, low-relief tundra-steppe landscape (Ager, 2003; Monteath et al., 2021) likely promoted the formation of low-lying waterlogged wetland environments prior to complete inundation by the rising seas. This has been well studied for the Doggerland

region in the North Sea, which was inundated during deglacial to Early Holocene sea-level rise (Blumberg et al., 2022; Gaffney and Fitch, 2022). However, neither the potential size of these Beringian coastal wetland areas, nor the geochemical implications of this transition have been investigated.

We assess changes in sea-level and CH_4 flux over the past 20,000 years to fully cover the last deglaciation from the end of the LGM to present. At 20,000 years BP, the Beringian landmass, bounded by the Laurentide and Cordilleran Ice sheet in the East, was defined as 'Mammoth steppe' (Guthrie, 2001) or 'Steppe-tundra', a graminoid-herb and dwarf-shrub dominated landscape indicating a cold and arid climate (Ager, 2003; Elias and Crocker, 2008; Yurtsev, 2001). However, Elias and Crocker (2008) suggest that a mesic shrub-tundra belt existed between the eastern and western steppe-tundra parts of Beringia and likely acted as ecological barrier between the Alaskan and Siberian part of Beringia (Elias et al., 1997; Elias and Crocker, 2008; Guthrie, 2001; Hoffecker et al., 2020). Edwards et al. (2000) indicate that Beringia was a tundra landscape but dominated by various types of vegetation forming a mosaic of tundra types at 18,000 yrs BP. Numerous paleo-river systems were crossing these flat shelves and extended the modern large rivers including the Khatanga, Anabar, Olenek, Lena, Yana, Indigirka, Kolyma, Yukon, Kobuk, and Noatak (Kleiber and Niessen, 1999; MacManus et al., 1974).

During the Bølling-Allerød warming (14,700 to 12,900 yrs BP), vegetation in Beringia changed. Pollen data indicate a birch-heath-graminoid tundra with peat-forming sedges and mosses (Ager, 2003; Elias et al., 1997). The warmer and wetter climate led to a northwards migration of shrubs, and trees and became favorable for the formation of peat (Monteath et al., 2021). Subsequently, during the Younger Dryas (12,900–11,700 yrs BP) the climate became drier and colder, but the vegetation was not uniform among Beringia (Ager, 2003). In west Beringia *Duscheckia* spp., *Salix* spp. and *Betula* spp. were present, whereas East Beringia saw an increase in *Populus* spp. and *Salix* spp. This might indicate that the climate was not colder in northeastern Beringia and could have allowed the increase in *Populus* spp. instead (Ager, 2003; Edwards et al., 2005). Deglacial sea-level rise inundated large parts of Beringia until the Early Holocene. Throughout the early Holocene, *Picea* and *Alnus* spread from interior Alaska north and westwards in east Beringia (Ager, 2003; Anderson, 1988) and *Picea* and *Pinus* trees became abundant in west Beringia (Edwards et al., 2005). The vast unglaciated, low-lying Beringian plain transformed from a rather dry steppe-tundra into a mesic and peat-favorable landscape before it became inundated by the rising sea-level. This is, however, only a broad generalization drawn from the few existing records, and Beringia was likely much more diverse and consisted of a mosaic of different landcover types as it spanned more than 1000 km in north-south and 2000 km in east-west direction.

3. Materials and methods

We estimated the CH_4 flux contribution of Beringian coastal wetlands by combining different data sets and methodologies, which are described in detail in the following sections. The basis for the flux estimation is the upscaling of areal CH_4 flux rates ($\text{g CH}_4 \text{ m}^{-2} \text{ yr}^{-1}$) with the area estimates of coastal wetlands. This is done in 1000-year time steps from 20,000 yrs BP to present. CH_4 flux rates are based on literature values and new CH_4 flux data from present-day northern hemisphere coastal wetlands (see Supplementary Material Fig. S2). The extent of coastal wetlands (for each time step) is based on a detailed GIS analysis including multiple data sets. First, paleo bathymetry grids from the PaleoMIST 1.0 model (Gowan et al., 2021) were used to estimate the timing of flooding. These grids were created using a glacial isostatic adjustment model that calculated the sea level equation. Then, timing of flooding was validated by terrestrial, inundated terrestrial sediments from Beringia (Supplementary Material Table S1). In a final step, the coastal wetland area was estimated and classified with the present-day

wetland map by Clewley et al. (2015). Therefore, this study is a combination of present-day analogs (CH_4 flux data and Alaska wetland map) with an extensive GIS analysis in order to estimate the magnitude of potential CH_4 fluxes from coastal wetlands in the past.

3.1. Modelled timing of inundation

To estimate the timing of flooding, we included all the non-glaciated terrain below current sea-level that went through a transgression from inland terrestrial to coastal wetland to marine environment (Fig. 1). We disaggregated this area into four regions – *Bering*, *Chukchi*, *Beaufort*, and *Laptev/East Siberian seas* – in order to examine regional differences in the timing of flooding (see Supplementary Material Fig. S1). We used the PaleoMIST 1.0 (Gowan et al., 2021) model output for the Beringian region in order to estimate the area and timing of flooding. PaleoMIST 1.0 is a glacial isostatic adjustment-based paleo topographic reconstruction model that includes relative sea-level and paleo bathymetry as an output. The model was created to estimate the sea-level contribution of the global ice sheets and is validated using observations of relative sea-level change. The PaleoMIST 1.0 raster data sets we use have a temporal resolution of 2500 years resulting in nine different grids (20,000 yrs BP to present) with a pixel size (spatial resolution) of 5000 x 5000 m.

The paleo bathymetry grids were used to calculate the timing of flooding, the location of the coastline for each time step and the area of coastal wetland for each time step. We calculated these parameters in 1000-year timesteps by raster analyses in ArcGIS 10.8 from 20,000 yrs BP to present (0 yrs BP). First, we calculated the linear increase (or decrease) for each pixel between two sequential PaleoMIST grids to establish grids for every 1000 years. In addition, we calculated the timing of flooding for each pixel, again by assuming a linear transition between two sequential grids. The timing of flooding was then determined as the point in time when a pixel elevation value relative to sea-level switched from positive (>0 ; above sea-level) to negative (<0 ; below sea-level). These two procedures allowed us to estimate the area which became flooded in each 1000-year time interval.

3.2. Raster analysis for estimating the size of coastal wetlands

To calculate the area of potential coastal wetlands for each timestep, we extracted the area for each 1m altitudinal step above the zero-line (coastline) until 10 m a.s.l. The altitudinal range of 0–10 m a.s.l. was chosen in order to set an altitudinal boundary for coastal wetlands which is often used as reference for defining coastal systems, e.g. in the IPCC report to evaluate exposure to sea-level rise (Wong et al., 2014) or by the United Nations (UNFCCC, & IUCN, 2022). This resulted in 10 different area estimations for potential coastal wetlands. However, we did not assume the entire area as uniform coastal wetland. We classified the potential wetland area of coastal Beringia using a present-day wetland map of Alaska (Clewley et al., 2015) as an analog. Based on the fraction of present-day wetlands found in coastal regions in Alaska, we sub-divided the wetlands in Beringia to have a more stratified estimation of coastal wetlands. Clewley et al. (2015) mapped the modern wetlands of Alaska using a combination of L-band ALOS PALSAR satellite data and topographic information and classified the wetlands according to the classification scheme given in Table S2 (as originally defined by Corrardin et al., 1979). We used this classification, which has a 50-m spatial resolution, for a stratification of the coastal wetland areas. Therefore, we first extracted the coastal area of present-day Alaska in 1-m altitudinal steps to 10 m a.s.l., based on the ARDEM version 2.0 with 1 km spatial resolution (Danielson et al., 2011). We then intersected the coastal areas with the wetland classification by Clewley et al. (2015) in order to retrieve the spatial extent of wetlands in the coastal zone of Alaska. This resulted in the coverage of each wetland type within the coastal zone for every 1m altitudinal interval. In a final step, this spatial ratio of wetland class coverage (Supplementary Material Table S2) was

applied to the Beringian coastal zones in order to estimate the area and type of coastal wetland. This present-day analog of wetland distribution in Alaska gives us an approximation of the potential coastal wetlands present during the flooding of Beringia and was used to calculate the potential coastal wetland area and CH₄ flux in Beringia for each time step.

3.3. Evaluation of flooding scenarios

The estimated flooding dates for each pixel derived from the paleo bathymetry grid analysis were compared to existing marine sediment cores from the flooded Beringia area that contained terrestrial sequences (Supplementary Material Table S1; Bauch et al., 2001; Elias et al., 1996; Hill et al., 1985, 1993; McManus and Creager, 1984; Nelson and Creager, 1977; Solomon et al., 2000) that were flooded due to sea level rise. We compiled a data set with existing radiocarbon (¹⁴C) dates, where

terrestrial peat was dated. We calibrated the ¹⁴C dates with IntCal 20 (Reimer et al., 2020) provided at calib.org (Reimer and Reimer, 2022) and separated the ¹⁴C dates in two groups; the first group contains cores with ¹⁴C dates for the top layer of terrestrial sediment indicating the time when the terrestrial sediment was flooded (or eroded) and covered by marine sediments. In any case, the date of this terrestrial top peat layer must be older than the estimated flooding by our model in order to agree with our model. The second group of cores contained terrestrial peat, which was dated somewhere in the middle or bottom of the peat layer. With these ¹⁴C dates, we could not extract exact information when this location was flooded and therefore the validation must be regarded with caution; however, we know that this terrestrial peat was certainly not flooded when it accumulated. Our rationale behind this evaluation is the assumption that no terrestrial peat formation occurred after flooding (e.g. Shennan, 1982), so all the peat dates should be older than the date of flooding indicated by our GIS analysis. Previous studies used the same

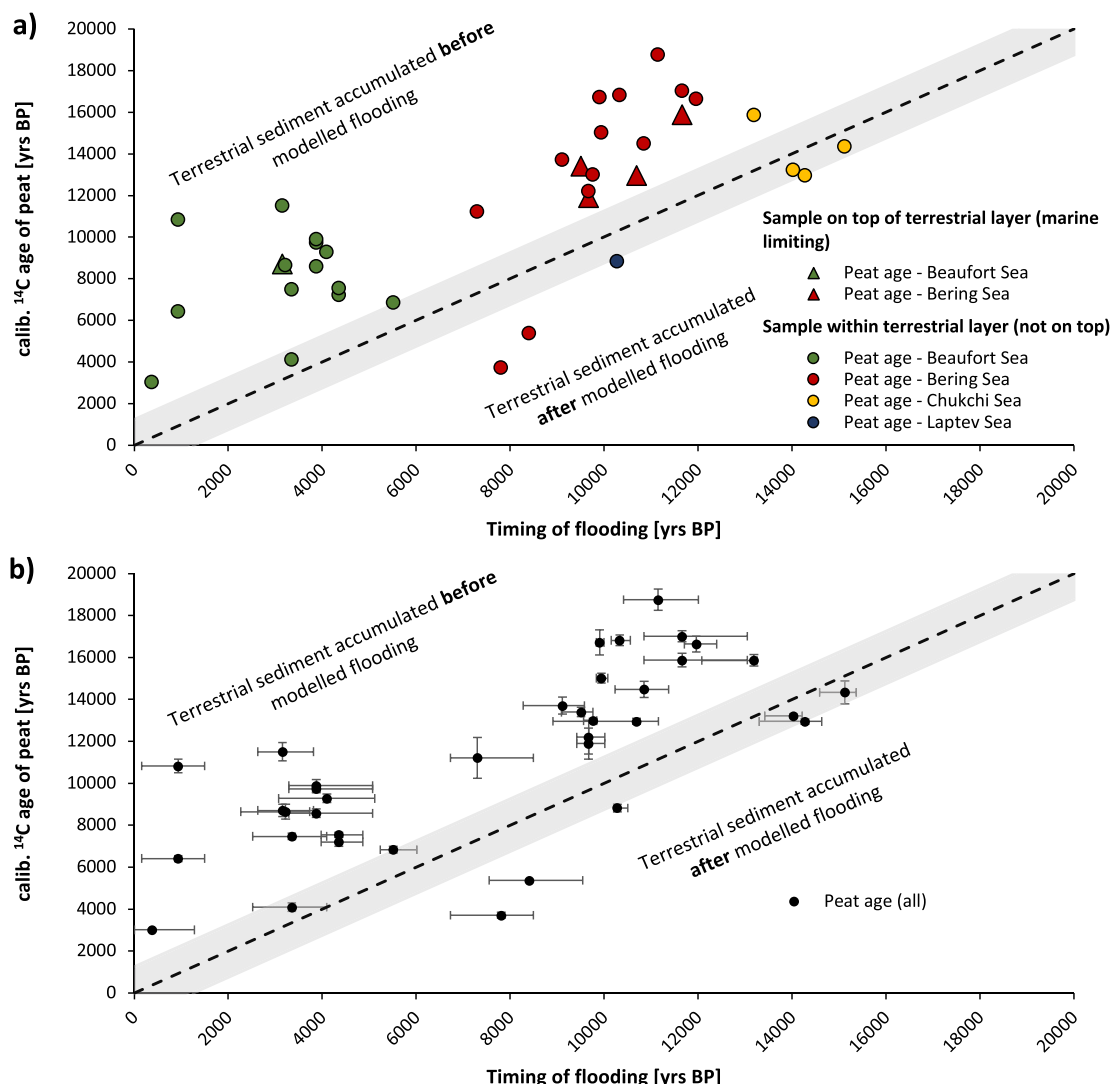


Fig. 3. Evaluation of the flooding model. a) Qualitative evaluation of modelled inundation times based on ¹⁴C dates from terrestrial sediments of the present-day marine Beringia domain. All points above the dashed line show that the terrestrial sediment (peat) was deposited before each location was inundated from sea-level rise and therefore support the model. The grey area shows an uncertainty of 2500 years, which is caused by the paleo bathymetry grids with a temporal resolution of this time frame. All points below the dashed line indicate that the peat formed after flooding of a particular location, which we consider not possible and therefore indicate that either the model does not perform well at this location or that the ¹⁴C date is showing a younger age that does not reflect a transition from terrestrial to marine sediments (data for this evaluation are presented in Table S1 in the supplementary material). b) Same validation points as in Fig. 3a with error bars. Horizontal error bars indicate the uncertainty of the location of the point by assuming an inaccuracy of the coordinates by $\pm 0.1^\circ$. Vertical error bars show the uncertainty of the calibrated ¹⁴C date. The grey area shows an uncertainty of 2500 years, which is caused by the paleo bathymetry grids with a temporal resolution of this time frame.

approach for inferring the flooding of a terrestrial landscapes (e.g. Törnqvist et al., 1998; Turner et al., 2010; Hijma and Cohen, 2019), determining the age of lake formation (e.g. Farquharson et al., 2016; Lenz et al., 2016) or date lake drainage events (e.g. Hinkel et al., 2003; Jones et al., 2012) by ^{14}C dating the stratigraphic transition in sediment cores. In total, we compiled 39 ^{14}C dates available for the Chukchi, Bering, Beaufort and East Siberian Seas. This allowed a qualitative analysis of the modelled times of flooding and allows us to check how accurate our flooding model is behaving in certain locations of the study area (see Fig. 3, model evaluation).

While the evaluation generally shows good agreement with the model, it also shows that parts of the Chukchi Sea might have been flooded about 1000 years later than what our model indicates. The mismatch could be because the exact spatial locations of the Chukchi sediment cores are uncertain due to rough coordinate denomination with none or only one decimal. Therefore, for some of these data, the coordinate information is very coarse (nearest degree). This can lead to a significant error of the positioning of a particular point. An uncertainty or inaccuracy of $\pm 0.1^\circ$ in longitude and $\pm 0.1^\circ$ in latitude can lead to an error of ± 4.5 km (longitude) and ± 11 km (latitude) at 67°N (for uncertainty of the ^{14}C data points, see Fig. 3b, which shows the data of Fig. 3a with error bars based on a $\pm 0.1^\circ$ deviation). Other sources of uncertainty is the coarse time resolution of PaleoMIST 1.0, and that locations in the Chukchi Sea may be sensitive to ice sheet history that is not captured in the model (e.g. Pico et al., 2020). Overall, this qualitative assessment by including ^{14}C dated terrestrial sediments shows that our sea-level rise model can be seen as a realistic approximation of the flooding of Beringia.

3.4. Methane flux data set

For upscaling CH_4 flux estimates in Beringia during the past 20,000 years, we collected 231 present-day CH_4 fluxes from coastal wetlands in the Northern Hemisphere (see Supplementary Material Table S3). We combined our own flux data from the Kenai Peninsula, Alaska (see section 3.5) with previously published data. Data were compiled from different sources (e.g. Treat et al. (2018, 2021); Poffenbarger et al. (2011); Liikanen et al. (2009); Holmquist et al. (2018)). CH_4 fluxes were calculated in $\text{g CH}_4 \text{ m}^{-2} \text{ yr}^{-1}$ for the growing season, which we set to 153 days (May 1 to September 30). The sources for the CH_4 fluxes used as input for the upscaling are listed in the Supplementary Material Table S3 and in Fig. S2. Each CH_4 data entry was harmonized by classifying it into one of the six wetland types (see Table S2). This resulted in a stratified pool of CH_4 fluxes and allowed a bootstrapping approach to estimate uncertainty in the CH_4 fluxes based on the variability of CH_4 fluxes associated to the different wetland types.

3.5. Methane flux measurements

In addition to the literature compilation of CH_4 fluxes, we measured CH_4 fluxes during a field campaign in August 2021 on the Kenai Peninsula, Alaska. We chose locations in coastal wetlands along transects to cover a gradient from freshwater flooded into tidal, saltwater flooded wetlands. In total, we measured at 27 different locations including saltwater tidal regularly flooded bare grounds, temporarily irregularly flooded, as well as seasonally flooded, vegetated coastal wetlands.

Flux measurements were made with a micro-portable LosGatos greenhouse gas analyzer (LosGatos Research) and a light-weight custom-made bucket chamber consisting of non-transparent PVC (diameter = 26 cm, volume $\sim 19,000 \text{ cm}^3$). We chose this small, lightweight equipment in order to be highly mobile in muddy, shrubby terrain and measure at field sites, which were not easy to access. At each site we measured three replicates for 7–10 min, described the vegetation cover (if present), and measured the chamber and air temperature. The bucket chamber was equipped with a venting tube and a small fan to

have well-mixed conditions in the chamber.

The CH_4 flux (in $\text{mg CH}_4 \text{ m}^{-2} \text{ h}^{-1}$) for each replicate measurement was calculated based on the volume and temperature of the bucket chamber, and the ideal gas law. We manually removed the first 30 s of each measurement, because of potential disturbance while placing the bucket chamber on the site (we did not use pre-installed collars). Fluxes were calculated by applying a linear regression to the CH_4 concentration and were given in $\text{mg CH}_4 \text{ m}^{-2} \text{ h}^{-1}$. The r-squared was used to determine the quality of the linear regression. Fluxes that had a linear regression with a r squared below 0.9 were discarded. However, we did not want to exclude all the near-zero measurements as these indicate important data as well (no CH_4 fluxes). Therefore, all measurements, which were below the precision of the greenhouse gas analyzer of 0.5 ppb ($\sim 0.44 \text{ mg CH}_4 \text{ m}^{-2} \text{ h}^{-1}$, depending on chamber volume) were included in the analysis as zero fluxes.

In a final step, we averaged all the replicates from a measurement site in order to have one CH_4 flux value per measurement site and calculated the CH_4 flux for the growing season of 153 days in $\text{g CH}_4 \text{ m}^{-2} \text{ yr}^{-1}$, which served as input data for the bootstrapping of the Beringia coastal wetland CH_4 estimation. Mean CH_4 fluxes for the measured sites are available on PANGAEA with the following link: <https://doi.org/10.1594/PANGAEA.960156> (Fuchs et al., 2024b).

3.6. CH_4 flux calculation for Beringia

We upscaled the CH_4 fluxes to Beringian coastal wetlands from point measurements to the entire area by multiplying the means of the observed fluxes with the means of the coastal wetland area for each time step resulting in an average total CH_4 flux in $\text{Tg CH}_4 \text{ yr}^{-1}$ in accordance to Treat et al. (2021). This approach included a two-way bootstrapping approach in order to capture the considerable uncertainty in both main input variables (CH_4 flux rates and coastal wetland area estimation) but reduce the impact of extreme values in our small datasets. In a first step, we bootstrapped the coastal wetland area for each time step by resampling the different area estimations based on the altitudinal intervals. We executed a bootstrapping with 5 samples (i.e. five different area estimations) and 100 iterations with replacement according to Jongejans and Strauss (2020), with the 95% confidence interval as the uncertainty range. This was executed for each time step from 20,000 to 0 yrs BP. In a second step, we bootstrapped the CH_4 fluxes according to the wetland classes. Since the CH_4 fluxes of the three classes *Temporarily irregularly flooded*, *Permanently to semi-permanently flooded*, and *Seasonally flooded* were not statistically significantly different (see Supplementary Material Fig. S4), these three classes were merged into one single class for the upscaling. Nevertheless, the input data were variable within each wetland class (Fig. S4); to better capture this variability, we used the bootstrapping approach rather than a simple median or mean for each wetland class. We executed a bootstrapping of 10 samples and 1000 iterations with replacement. Again, the 95% confidence interval was chosen for an uncertainty estimation. In a final step, we upscaled the CH_4 fluxes to Beringian coastal wetlands by multiplying the bootstrapped mean of CH_4 fluxes with the mean of the coastal wetland area for each time step of 1000 years. The uncertainty of the final estimation was calculated through error propagation according to Taylor (1997). This approach includes the variability in both input parameters, and therefore provides an estimation with uncertainty of Beringian coastal wetland CH_4 flux contribution for the past 20,000 years based on present-day data sets.

4. Results

4.1. Spatio-temporal dynamics of the flooding of Beringia

The flooding history of Beringia was reconstructed from geospatial analysis of the paleo bathymetry grids and a model-based sea-level reconstruction specifically for Beringia (Fig. 2). Of the total Beringian

shelf area, 44% is located in the East Siberian and Laptev Seas and 44% in the Chukchi and Bering Seas combined (Fig. 2a). At 12,000 yrs BP, more than half of Beringia (52%) was already flooded, but the time interval with the largest area flooded occurred during 12,000–11,000 yrs BP when more than 300,000 km² (or 11% of total study region) were flooded within 1000 years. By 7500 BP, the remaining exposed Beringian shelf was almost entirely in the Beaufort Sea (Fig. 2f). With the slower rate of sea-level rise in the last 5000 years, only 126,500 km² (or 4%) of Beringia were flooded, with the majority of that happening in the Beaufort Sea (72,100 km²).

There were clear differences in the timing of flooding for the various regions (Fig. 2 and Supplementary Material Fig. S3). For example, large areas of the Chukchi Sea were flooded between 17,000 and 12,000 yrs BP, while most of the Beaufort Sea was flooded no earlier than 9000 yrs BP. This heterogeneity was mostly due to the different topographical characteristics (e.g., the vast, flat Laptev and East Siberian Shelf) and differences in relative sea-level rise due to isostatic adjustments (e.g., the proximity of the Beaufort Sea to the melting Laurentide Ice sheet and the associated forebulge collapse and glacial isostatic adjustment effects (Gowan et al., 2021) (see Supplementary Material Fig. S3). Between 16,000 yrs BP and 9000 yrs BP, 250,000 km² or more were flooded each millennium (Fig. S3). While the flooding in the first period (20,000–14,000 yrs BP) was dominated by flooding of the Chukchi and Bering Sea, the flooding in the second period (13,000–7000 yrs BP) was dominated by the flooding of the large East Siberian and Laptev Sea shelf (Fig. S3).

We found generally good agreement between modelled flooding times and ¹⁴C dates of terrestrial sediment in sea-floor cores (Fig. 3a) with the exception of two data points in the Bering Sea. The majority of the points were consistent with the inferred timing of flooding, especially for the Bering and Beaufort Sea. However, some ¹⁴C dates appear to be significantly older than the inferred flooding. This could be caused by either erosion (e.g. the top terrestrial organic material and permafrost was eroded prior to or during flooding) or the dated organic material was not the upper limit of the terrestrial environment. In addition, the model output and the ¹⁴C dates did not align as well for the Chukchi Sea. The evaluation shows that parts of the Chukchi Sea might have been flooded about 1000 years later than what our model proposed.

4.2. Coastal wetland area and CH₄ emissions since 20,000 yrs BP

The extent of present-day coastal wetlands in this region gives an indication of the potential extent of coastal wetlands in the past by

assuming similar topographical profile conditions. The mean ($\pm 95\%$ CI) bootstrapped coastal wetland area for Beringia (Fig. 4a) varies between a mean value of 110,000 km² (7000 yrs BP) and 260,000 km² (14,000 yrs BP) and is consistently larger than 200,000 km² during 16,000–10,000 yrs BP, indicating that from the Bølling-Allerød to the Early Holocene, large areas of Beringia were close to or at sea-level. This is important to consider for biogeochemical processes, since the timing of major climatic changes (Bølling-Allerød warming, Younger Dryas cooling, Early Holocene warming) coincides with a large area transitioning from a terrestrial to a coastal to a marine environment, changing the nature of carbon cycling. When taking the maximum potential wetland area within the 0–10 m a.s.l. altitudinal range, the size of coastal wetlands would nearly double (dashed line in Fig. 4a), and could have been as large as 450,000 km² at 15,000 yrs BP.

Based on the mean area of coastal wetlands, and the inclusion of a wide range of CH₄ flux data representing 231 CH₄ measurements from 72 different wetland locations covering six major coastal wetland classes in the Northern Hemisphere (see Methods and Fig. S2), we estimated the total CH₄ flux from Beringia for each 1000-year time interval. This analysis results in a maximum CH₄ flux of up to 3.5 (+4.0/−1.9) Tg CH₄ yr^{−1} at 14,000 yrs BP. The analysis shows a high CH₄ flux of 2.5–3.5 Tg CH₄ yr^{−1} from 16,000 to 9000 yrs BP for coastal wetlands of Beringia (Fig. 4b). The beginning (20,000–17,000 yrs BP) and end (8000 – present) of the studied period are characterized by lower fluxes from Beringian coastal wetlands with a flux of less 2 Tg CH₄ yr^{−1}, which is caused by the smaller area covered by coastal wetlands. The bootstrapped mean CH₄ flux for Beringian coastal wetlands is 13.3 (+14.0/−8.4) g CH₄ m^{−2} yr^{−1} based on contemporary analogs. The estimations of total fluxes include an uncertainty estimation for both the area and flux rates, which results in a total uncertainty of approximately +106/−63% (Fig. 4b), which stems primarily from the wide range of the CH₄ fluxes, which is three times as large as the uncertainty of the area estimation and indicate that more CH₄ flux data is needed to reduce the uncertainty in the estimations.

5. Discussion

5.1. Flooding and coastal wetlands of Beringia

By estimating the timing of flooding for all of Beringia and not only the Bering Land Bridge, we show that spatial extent and time of flooding varies for the different regions of Beringia (Fig. 2). In addition, we

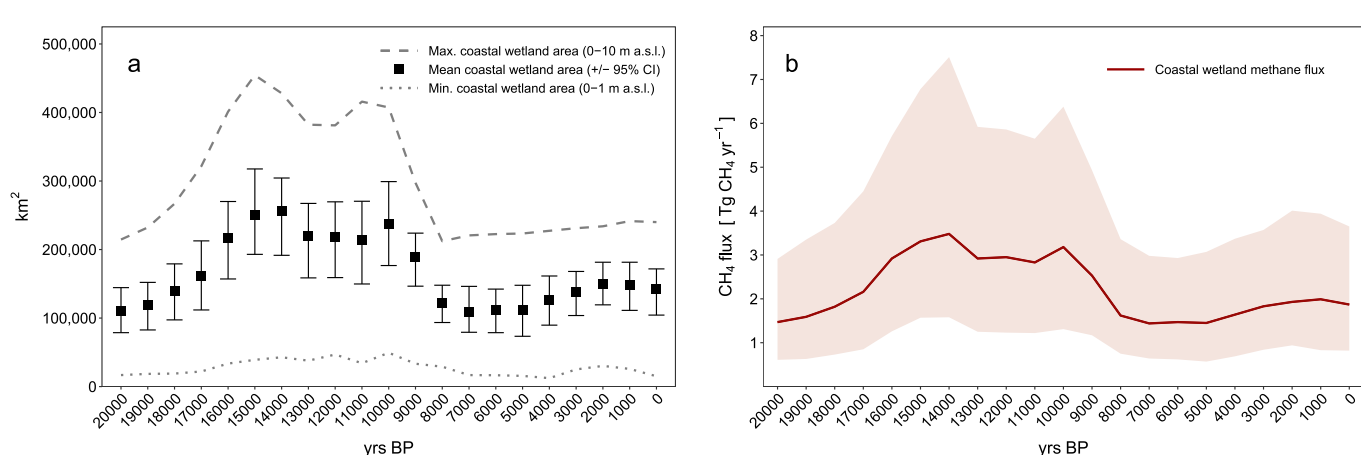


Fig. 4. Coastal wetland area and CH₄ flux for the past 20,000 years. **a)** Estimates of coastal wetland areas of Beringia, based on a bootstrapping approach of contemporary coastal wetlands at 1000-year time intervals. The dashed line indicates the maximum potential wetland area, and the dotted line indicates the minimum potential wetland area. The maximum and minimum area estimates were calculated without bootstrapping. **b)** Total CH₄ fluxes of coastal wetlands in Beringia for the past 20,000 years based on mean coastal wetland areas. Red line is the mean bootstrapped CH₄ flux in Tg CH₄ yr^{−1} with the 95% confidence interval (red area). The confidence interval (red area) includes the uncertainty of both input values, CH₄ flux rates and wetland area estimation.

estimate the area of coastal wetlands for the past 20,000 years, which was more than 200,000 km², during the period of 16,000–9000 yrs BP, and therefore in the same order of magnitude as the present day wetland area in Alaska according to [Pastick et al. \(2017\)](#) with 177,000 km². When comparing it to contemporary coastal wetlands of Alaska (84,500 km², 0–10 m a.s.l.), coastal wetlands of Beringia always covered a larger area during the past 20,000 years. The potential current coastal wetland area for the Russian part of the study area is also on the lower end with 125,700 km² (which is 81% of the area 0–10 m a.s.l. according to the MERIT DEM ([Yamazaki et al., 2017](#)) in combination with a very rough wetland map from Russia (Land resources of Russia – Wetlands map ([Stolbovoi and McCallum, 2002](#))). However, our approach is an approximation of past conditions. In particular, using the extent of present-day Alaskan coastal wetlands as an approximation to past Beringian coastal wetlands assumes similar topographic gradients lead to similar past wetland extent, despite differences in climate and geomorphic setting. For example, the East Siberian and Laptev Sea shelves likely consisted of Yedoma deposits ([Strauss et al., 2021](#)), whereas present day-coastal areas in Alaska are a mix of low lying (thermokarst-affected) regions on the Arctic Coastal Plain and the Yukon-Kuskokwim Delta, more hilly shorelines along the Chukchi Sea and Kenai Peninsula, and Yedoma deposits on the Seward Peninsula. In addition, our model does not consider any sediment erosion or deposition processes and does not include microtopography. With our spatially coarse, 5 × 5 km resolution grid, we are not able to make statements on local surface changes such as permafrost thaw settlement, lake formation or erosional river valleys ([Brosius et al., 2021](#)), particularly within a likely Yedoma environment that might have existed in parts of Beringia ([Strauss et al., 2021](#)). We are aware that this can lead to inaccurate estimations of flooding times but given the coarse spatial and temporal resolution and limited data on past conditions in Beringia, our approach is a promising attempt to understand the processes in Beringia that influence CH₄ flux with sea-level transgression, which have not yet been quantified. These results highlight the importance of including these areas for estimating the CH₄ flux contribution to atmospheric CH₄ during the past 20,000 years.

Our coastal wetland and timing of flooding estimations are generally consistent with constraints based on ¹⁴C-dated sediment cores ([Fig. 3](#)), although uncertainties remain and the ¹⁴C dates have to be considered with caution. In particular, two locations in the Bering Sea show a large deviation from the model. Both points are located in the greater Yukon-Kuskokwim Delta region and might therefore be affected by fluvial sediment deposition and can therefore be considered as outliers. Additional uncertainties for the timing of flooding in the Chukchi Sea arise from two main factors. First, the linear interpolation between the PaleoMIST paleo bathymetry grids introduces uncertainty due to their coarse temporal resolution of 2500 years. Second, it is plausible that an early inundation estimated for coastal lowlands of the Chukchi Sea region is a result of the choices made when constructing the PaleoMIST model. The paleo bathymetry grids were determined using glacial isostatic adjustment (GIA). The GIA model ([Gowan et al., 2021](#)) utilizes only a single, three layer, radially symmetric Earth structure with a 120 km elastic lithosphere and contrasts in viscosity only between the upper and lower mantle at 660 km depth. In reality, the Earth has a 3D viscosity structure ([Li et al., 2022](#)). This may be an issue, since the Earth structure between the area covered by the Cordilleran Ice Sheet, which overlies a region undergoing active tectonics, is different than the Laurentide Ice Sheet, which overlies a more stable cratonic area. Beringia is close enough to these ice sheets that it may require this contrast to be included to accurately model the sea-level. The Chukchi Sea area is also in the intermediate field of these ice sheets, and the calculated sea-level there is sensitive to the choice of mantle viscosity ([Gowan et al., 2021; Pico et al., 2020](#)). Modelling relative sea-level in the intermediate field is complicated ([Dyke and Peltier, 2000](#)), and has been a problem when trying to model the paleo sea-level along the United States East Coast ([Engelhart et al., 2011](#)). Nevertheless, by comparing PaleoMIST results

to those of ¹⁴C-dated terrestrial sediments from cores from the Beringian shelf, we find good agreement. The consistency between our estimated time of flooding and ages of terrestrial deposits in sediment cores lends validity to our results ([Fig. 3](#)). In summary, by including paleo bathymetry grids from the Bering region, we were able to infer the timing of flooding more accurately for the different sub-regions of Beringia and calculate the area of coastal wetlands for the past 20,000 years.

In terms of the breaching of the Bering Land Bridge, our study indicates an early inundation compared to other studies (e.g., [Jakobsson et al., 2017](#)). Our model infers that the Bering Land Bridge was inundated approximately 12,500 yrs BP. The reason for this early flooding estimate might be the spatial resolution of the grids. With 25 km² pixel size the accuracy is very coarse and therefore uncertain for determining the exact timing of the breaching of the Bering Land Bridge. Also, the temporal resolution of the grids (2500 years) introduces some uncertainty; however, for the grid of 12,500 yrs BP the Bering Land Bridge was already inundated. Our suggested time of flooding of the Bering Land Bridge is therefore early compared to a proxy-based reconstruction from the Chukchi Sea by [Jakobsson et al. \(2017\)](#) but fits into the time range provided by the standstill theory proposed in a modeling study by [Pico et al. \(2020\)](#) and is in accordance with [Elias et al. \(1992\)](#) and [England and Furze \(2008\)](#).

5.2. Beringia CH₄ flux estimates in a broader context

Our estimated CH₄ fluxes are based on present-day analogs of CH₄ fluxes and coastal wetland classification, as well as paleo bathymetry grids from the PaleoMIST 1.0 model ([Gowan et al., 2021](#)). This is, to our knowledge, the most feasible approach so far to estimate past terrestrial CH₄ fluxes from an inundated area. One strength of our model is the inclusion of a wide range of CH₄ flux data representing 231 CH₄ measurements from 72 different wetland locations in the Northern Hemisphere (see [Fig. S2](#)). This data covers six main wetland classes according to [Clewley et al. \(2015\)](#) including saltwater tidal regularly flooded, temporarily irregularly flooded, permanently/semi-permanently flooded, non-tidal saturated and water bodies. This data set was used as input data for the upscaling based on a bootstrapping approach, contributing to a wide range of uncertainty ([Fig. 4b](#)) but capturing the most likely scenarios. However, we are aware that coastal CH₄ fluxes are more complex and are for example dependent on temperature ([Rinne et al., 2018](#)), salinity ([Poffenbarger et al., 2011](#)) as well as they can have seasonal, weekly or even daily fluctuations ([Shurpali et al., 1993; Rosentreter et al., 2018; Roth et al., 2022](#)). This leads to a large uncertainty for the upscaled results and the need for more high-resolution CH₄ flux data, especially from northern high-latitude coastal wetlands. [Roth et al. \(2022\)](#) show that about 50 CH₄ concentrations samples per day are necessary in order to resolve the different drivers of variability and to significantly improve the validity of the results. Unfortunately, these data are not yet available for northern coastal wetlands.

We consider our CH₄ flux estimates (1.4–3.5 Tg CH₄ yr⁻¹) to be conservative and at the lower end of what can be expected for coastal wetlands of Beringia, because we only estimate CH₄ fluxes for a growing season of 153 days with zero fluxes during the remainder of the year. A prolongation of the growing season and/or assuming minor fluxes during the winter period (e.g. [Treat et al., 2018](#)) would increase the annual fluxes from coastal wetlands of Beringia. In addition, our approach assumes coastal wetlands within 0–10 m altitudinal intervals, but we might underestimate the true size of coastal wetlands. If we assume coastal wetlands to occupy the entire area up to 10 m a.s.l. (thus, not applying the bootstrapping for the coastal area on altitudinal intervals) and calculate the CH₄ fluxes with an average bootstrapped CH₄ flux of around 13.3 g CH₄ m⁻² yr⁻¹, which is lower compared to US freshwater wetlands (32.1 g CH₄ m⁻² yr⁻¹) or US saltwater dominated wetland fluxes (16.9 g CH₄ m⁻² yr⁻¹) ([Bridgman et al., 2006](#)), the maximum flux could be up to 6.0 Tg CH₄ yr⁻¹ at 14,000 yrs BP, which would nearly double the fluxes compared to our bootstrapped results. Importantly, the

CH_4 released from coastal wetlands is likely young $^{14}\text{C-CH}_4$ and therefore coastal wetlands could have been important sources contributing to the rapid increase of Northern Hemisphere atmospheric CH_4 concentration as indicated by previous studies (Dyonisius et al., 2020; Petrenko et al., 2017). The analysis of quantifying and modelling the absolute amount of $^{14}\text{C-CH}_4$ from ice cores by Dyonisius et al. (2020) and Petrenko et al. (2017) show the significance of contemporaneous CH_4 to the rapid increase of atmospheric CH_4 compared to geological CH_4 emissions during the Younger Dryas and therefore highlight the important role of wetlands for past (and present) CH_4 emissions.

Our flux estimates may also be conservative due to constraining the estimates to the now-inundated land area of Beringia, not accounting for wetland formation prior to becoming a coastal area resulting from thaw of ice-rich permafrost on the continental shelf (Romanovskii et al., 2000, 2004), and not accounting for wetland formation outside of the coastal zone as the climate warmed and became wetter (Monteath et al., 2021).

Nevertheless, coastal wetlands of Beringia were significant CH_4 sources. For comparison, present-day wetland emissions from North America were estimated to $9.4 \text{ Tg CH}_4 \text{ yr}^{-1}$ based on a soil database synthesis (Bridgman et al., 2006) and present-day CH_4 estimations for Alaskan wetlands range in the same order of magnitude as our study with $1.7 \text{ Tg CH}_4 \text{ yr}^{-1}$ (Bridgman et al., 2006) and $2.1 \text{ Tg CH}_4 \text{ yr}^{-1}$ (Treat et al., 2021). Therefore, our CH_4 flux estimate of $1.4\text{--}3.5 \text{ Tg CH}_4 \text{ yr}^{-1}$ is comparable to estimated fluxes of contemporary Alaskan wetlands. In addition, a process-based modelling estimated $0.9 \text{ Tg CH}_4 \text{ yr}^{-1}$ (McGuire et al., 2018), while a top-down estimate based on aircraft remote sensing resulted in a flux of 2.1 Tg CH_4 (Chang et al., 2014) for the growing season of Alaska. For comparison on a global scale, Saunois et al. (2020) estimated the global wetland CH_4 emissions to $101\text{--}179 \text{ Tg CH}_4 \text{ yr}^{-1}$ and Rosentreter et al. (2021a) estimated a CH_4 flux for coastal wetlands of $14.6 \pm 16.0 \text{ Tg CH}_4 \text{ yr}^{-1}$ indicating the high variability in CH_4 fluxes for coastal wetlands and the uncertainty in CH_4 upscaling attempts.

From an Arctic perspective, synthesis work was done by Olefeldt et al. (2021) and Kuhn et al. (2021) who established a dataset for areal extents as well as terrestrial and aquatic CH_4 fluxes in boreal and arctic ecosystems and found that water table position, soil temperature, and vegetation composition were major control factors for terrestrial ecosystem fluxes and water temperature, lake size and lake genesis were the main control factors for aquatic ecosystems. Treat et al. (2024)

estimated a CH_4 flux between 5.3 and $37.5 \text{ Tg CH}_4 \text{ yr}^{-1}$ from wetlands and lakes in the northern permafrost region highlighting the low density of observation in a highly variable landscape as a major challenge. A land cover based upscaling by Ramage et al. (2024) resulted in a mean annual CH_4 flux of $38 \text{ Tg CH}_4 \text{ yr}^{-1}$ for the northern permafrost region between 2000 and 2020 identifying spatial representation, length and quality of observational time series as major limiting factor for the upscaling. Also, the omission of non-growing season CH_4 flux can lead to an underestimation. Treat et al. (2018) estimated a non-growing CH_4 flux of $6.1 \text{ Tg CH}_4 \text{ yr}^{-1}$ for northern ecosystems. Albuhaiasi et al. (2023) modelled CH_4 emissions for the boreal and pan-arctic wetlands $>50^\circ\text{N}$ based on soil moisture data from satellite remote sensing and estimated $29.5\text{--}39 \text{ Tg CH}_4 \text{ yr}^{-1}$, including growing and non-growing season fluxes.

For a broader perspective and comparison to past fluxes, a CH_4 flux model output for the LGM resulted in $107 \text{ Tg CH}_4 \text{ yr}^{-1}$ (Kaplan, 2002) and $108 \text{ Tg CH}_4 \text{ yr}^{-1}$ (Valdes et al., 2005) for global wetlands and $23.3 \text{ Tg CH}_4 \text{ yr}^{-1}$ for Northern Hemisphere (extratropical) wetlands (Kleinen et al., 2020). At 10,000 yrs BP Kaplan et al. (2006) modelled a CH_4 flux of around $125 \text{ Tg CH}_4 \text{ yr}^{-1}$ for global wetlands and Kleinen et al. (2020) estimated $48.3 \text{ Tg CH}_4 \text{ yr}^{-1}$ for northern extratropical wetlands, which is only slightly higher than the CH_4 flux of coastal wetlands on Beringian shelves, northern peatlands and thermokarst lakes combined at 10,000 yrs BP (see Fig. 5).

5.3. Integrating coastal wetlands with other sources of CH_4 in the Northern Hemisphere

With a flux of around $3.3 \text{ Tg CH}_4 \text{ yr}^{-1}$ at the onset of the Bølling-Allerød, Beringian coastal wetlands contribute the same amount of CH_4 as thermokarst lakes and northern peatlands combined and contribute about 11–14% of emitted CH_4 during the early Holocene (Fig. 5). In the later stages, northern peatlands become the dominant source of CH_4 , mainly due to their much larger area. Combining these fluxes shows that CH_4 emissions from northern landscapes increased 10-fold from 16,000 to 9000 yrs BP (Fig. 5). Our study indicates that by including coastal wetland formation from the now-inundated continental shelf region of Beringia, the northern wetland contribution to the rise in atmospheric CH_4 concentrations started at around 17,000 yrs BP. The estimated fluxes were larger than thermokarst lakes (Brosius et al., 2012) until 15,

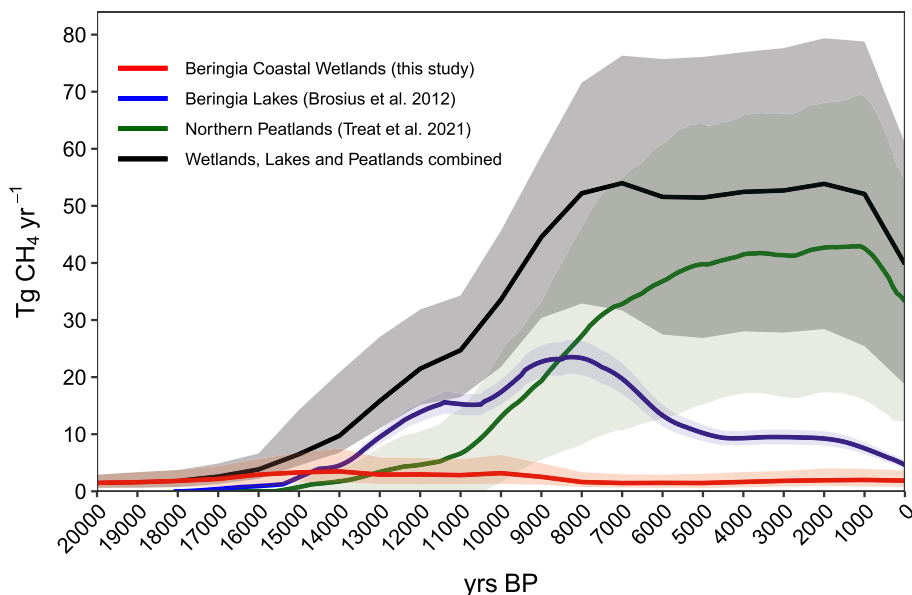


Fig. 5. Northern Hemisphere CH_4 fluxes. CH_4 fluxes from Beringia coastal wetlands (red) in comparison to thermokarst lakes in contemporary terrestrial Beringia (blue) and northern peatlands (green). The black line shows the sum of these three different domains (coastal wetlands, thermokarst lakes and northern peatlands) including the uncertainty range (grey area).

000 yrs BP and larger than peatlands until about 13,000 yrs BP (Treat et al., 2021). Nevertheless, the estimates presented here underrepresent the total potential continental shelf wetland CH₄ flux, as we only include Beringian coastal wetlands in our flux estimations, rather than the entire potential area for wetlands across Beringia, which encompasses a much larger area.

By comparing the flooded area of Beringia to the terrestrial, not flooded (non-coastal) areas for each time step (Fig. 6), there is a high potential for additional large wetlands (and increased CH₄ fluxes) particularly in the first quarter (20,000–15,000 yrs BP) of the investigated time period, when the terrestrial (not yet flooded area of the Beringian shelf) was up to 23-times larger than the area covered by coastal wetlands. If only a fraction of that vast area was occupied by wetlands, CH₄ fluxes from this region would have been considerably higher. There is for example some evidence that riverine channels and therefore likely riparian wetlands existed for the Laptev Sea and Bering Sea region (Kleiber and Niessen, 1999; MacManus et al., 1974). However, climate conditions at the end of the LGM were likely dry and cold (Ager, 2003; Guthrie, 2001) which might have restricted the formation of wetlands until the climate warmed and became wetter. Nevertheless, some indications based on pollen data for more abundant wetlands outside the coastal area suggest that at least between the eastern and western part of Beringia, a mesic shrub-tundra belt could have existed (Elias and Crocker, 2008; Guthrie, 2001; Hoffecker et al., 2020), and plant macrofossil studies indicate the local presence of aquatic and wetland plants (e.g. *Myriophyllum spicatum*, *Sphagnum* spp.) for the time period 20,000–14,000 yrs BP (Elias et al., 1997). This indicates that Beringia was not entirely a dry tundra-steppe during the deglaciation but consisted of a mosaic of different ecosystems with the possibility to have included CH₄-emitting wetlands. During the beginning of the Bølling-Allerød, Monteath et al. (2021) reported that the landscape became wetter and peat formation was more widespread, indicating the presence of wetlands in non-coastal Beringia. This is supported by biomarkers that point to wetter conditions and permafrost thaw in inland Beringia (Meyer et al., 2019). However, the estimation of the total area of wetlands in Beringia and their CH₄ fluxes is only speculative and outside the scope of this study.

While more wetlands outside the coastal domain were possibly present during the past 20,000 years in Beringia, other processes potentially have affected the total CH₄ fluxes from Beringia. During the deglaciation and warming of the climate, the previously unglaciated, permafrost-affected area was undergoing widespread change (Brosius et al., 2012, 2021; Pellerin et al., 2022). Thick ice-rich Yedoma deposits are common in some regions of the Beringian shelves (Gavrilov et al.,

2003; Romanovskii et al., 2000; Strauss et al., 2017, 2021), and thaw of ice-rich permafrost would have led to CH₄-emitting thermokarst lake landscapes (Brosius et al., 2012, 2021; Pellerin et al., 2022). In particular, biomarkers from marine sediment cores indicate that the flooding and rapid degradation of Beringian permafrost (Yedoma) deposits contributed to the rise in atmospheric CO₂ at 14,600 and 11,500 yrs BP (Meyer et al., 2019; Winterfeld et al., 2018). However, the contribution of permafrost thaw and Yedoma degradation to CH₄ fluxes prior and during the flooding of these Yedoma permafrost deposits is not quantified yet for Beringia. Evidence shows that permafrost thaw from thermokarst lake formation in Alaska and Siberia began as early as 18,000 yrs BP but did not substantially rise until 14,000 yrs BP (Brosius et al., 2012). While 850,000 km² of Beringia were flooded between 14,000 and 11,000 yrs BP, a vast area (~900,000 km²) was still a terrestrial (non-coastal) environment by 11,000 yrs BP (Fig. 6) where permafrost thaw and thermokarst processes likely expanded, resulting in increased CH₄ fluxes from these areas. For example, thermokarst lakes and low-lying drained lake basins formed before flooding and then transformed into thermokarst lagoons due to sea-level rise and coastal erosion (Angelopoulos et al., 2020; Jenrich et al., 2021; Romanovskii et al., 2004), with the potential to release CH₄ during further permafrost degradation of these deposits (Shakhova et al., 2019).

Our study explores the role of coastal wetlands from only the Beringian shelf, but other continental shelves likely also contributed. Beringia, which covers ~57% of the northern hemisphere exposed shelf area during the LGM, is not as heavily impacted by isostatic sea-level effects (except the rather small Beaufort Sea shelf) (Keigwin et al., 2006). Outside of the Beringian domain, other northern regions (such as the North Sea shelf or the Kara Sea shelf) provided a large potential area (about 1.3×10^6 km²) where thermokarst processes and (coastal) wetland formation have occurred. Presence of extensive wetlands were discovered for the North Sea shelf based on many marine cores and geophysical soundings finding wetland deposits starting to form around 13,700 to 10,700 yrs BP (Lippmann et al., 2021; Wolters et al., 2010).

To improve our understanding of the Beringian paleo-environment, collecting cores from the Beringian shelf that capture the marine-terrestrial transgression would help constrain the timing of flooding and help characterize past Beringian climate and landscapes not only for the Bering Land Bridge but also for the other regions of Beringia. Better characterization of Beringian paleoenvironments would help constrain paleo-coastal wetland CH₄ fluxes during the deglacial sea-level transgression.

Our estimations of the timing of flooding and potential CH₄ fluxes from coastal wetlands in Beringia highlight the importance for further investigating the processes on the Beringian shelf and its implications for past climatic changes. In this study, we show that inundation of Beringia and the associated time-transgressive development of coastal wetlands represent a hitherto unquantified Northern high latitude source of atmospheric CH₄ observed in ice core records. The fluxes from coastal Beringian wetlands pre-date thermokarst lake and peatland initiation within their modern ranges, indicating an earlier Northern high latitude source. With this first approximation of CH₄ fluxes for Beringian coastal wetlands, we show the significance of including these former terrestrial areas into estimations of past CH₄ sources as they shift the onset of Northern high latitude CH₄ fluxes from northern regions earlier towards the Bølling-Allerød. These results further suggest that the inundation of low-lying parts of the Arctic coastal regions with future increasing rates of sea-level rise could contribute to an increase of atmospheric CH₄.

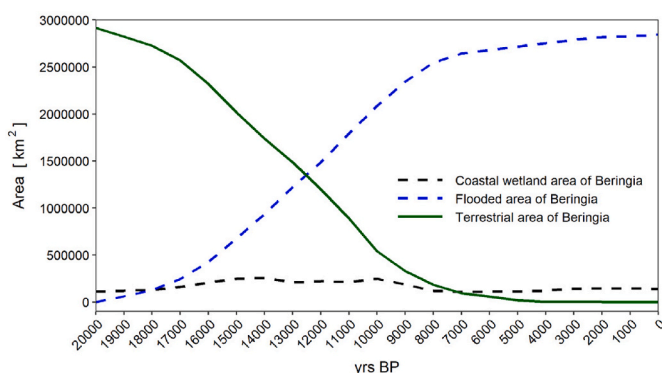


Fig. 6. Flooded vs. terrestrial area of Beringia. Ratio between flooded (blue dashed line) and terrestrial (green solid line) area of Beringia during the past 20,000 years. In addition, the (bootstrapped) coastal wetland area for Beringia is added as comparison (dashed black line). The terrestrial area includes all the non-flooded areas except the coastal wetland area. At 0 yrs BP, terrestrial area of Beringia is ~0, and the coastal wetland area is on current terrestrial land in Alaska and Russia.

6. Conclusions

The flooding of Beringia during the past 20,000 years led to a transition of vast lowland tundra landscapes first into coastal and then into marine ecosystems. We estimated for the first time the size of coastal wetlands in Beringia in 1000-year time intervals. In addition, we compiled a CH₄ flux data set for coastal wetlands and estimated the

potential CH₄ flux for coastal wetlands in Beringia during the past 20,000 years. This is the first characterization of CH₄ fluxes from coastal wetlands for the now inundated Beringian shelf. The results indicate that these areas contributed to overall Northern Hemisphere CH₄ concentration preceding other processes such as thermokarst lake development and peatland formation. In addition, our study shows that large areas in Beringia (consistently more than 200,000 km²) were close to or at sea level during the time from the Bølling-Allerød to the Early Holocene and therefore shifting from terrestrial to coastal and eventually into a marine ecosystem. This cascade from land to sea coincides with the timing of major climatic changes, and therefore likely had significant influences on the northern carbon cycle. With our study, we quantify a past previously overlooked CH₄ source and therefore add a missing piece to Northern Hemisphere CH₄ emissions estimates during the last Deglaciation.

Funding

National Science Foundation (NSF) ARC-1903623 (KWA, LB)
 National Science Foundation (NSF) ARC-1903735 (SF, CT)
 ERC H2020 Project FluxWIN 851181 (CT, MF)
 Helmholtz Impulse and Networking Fund (CT)
 AWI base funds for expeditions (CT, MF)
 Postdoctoral Fellowship of the Japan Society for the Promotion of Science (EJG)
 National Science Foundation (NSF) OISE-1927553 (BMJ)
 USGS Land Change Science/Climate Research and Development (MCJ)
 NPS Inventory & Monitoring Division (JAD)

CRediT authorship contribution statement

Matthias Fuchs: Conceptualization, Methodology, Investigation, Visualization, Input data sets, Writing – original draft, Writing – review & editing. **Miriam C. Jones:** Conceptualization, Methodology, Investigation, Writing – original draft, Writing – review & editing. **Evan J. Gowan:** Methodology, Input data sets, Writing – review & editing. **Steve Frolking:** Conceptualization, Methodology, Supervision, Writing – review & editing. **Katey Walter Anthony:** Methodology, Input data sets, Supervision, Writing – review & editing. **Guido Grosse:** Methodology, Supervision, Writing – review & editing. **Benjamin M. Jones:** Methodology, Writing – review & editing. **Jonathan A. O'Donnell:** Methodology, Writing – review & editing. **Laura Brosius:** Methodology, Input data sets, Writing – review & editing. **Claire Treat:** Conceptualization, Methodology, Investigation, Input data sets, Supervision, Writing – original draft, Writing – review & editing.

Declaration of competing interest

The authors declare that they have no known competing financial interests or personal relationships that could have appeared to influence the work reported in this paper.

Data availability

All data for this study are available on the PANGAEA data set repositories under the following links.

- Timing of flooding (raster data set) (Fuchs et al., 2024c): <https://doi.org/10.1594/PANGAEA.960150>
- Input data set, methane fluxes from coastal wetlands (Fuchs et al., 2024a): <https://doi.org/10.1594/PANGAEA.960160>
- Measured methane fluxes from coastal wetlands (Fuchs et al., 2024b): <https://doi.org/10.1594/PANGAEA.960156>

Acknowledgements

This study was supported by the National Science Foundation (NSF) – P2C2 Project (Paleo perspectives on climate change) project numbers ARC-1903623 and ARC-1903735. MF and CT acknowledge funding from ERC H2020 Project FluxWIN #851181 and the Helmholtz Impulse and Networking Fund. Fieldwork in August 2021 was supported by AWI base funds for expeditions. We thank the City of Kenai, Alaska and the Alaska Department of Natural Resources for field work permits in the Kenai region. EJG is funded by an International Postdoctoral Fellowship of the Japan Society for the Promotion of Science. Additional support was provided to BMJ through NSF award OISE-1927553, to MCJ through USGS Land Change Science/Climate Research and Development, and to JAD through NPS Inventory & Monitoring Division. Any use of trade, firm, or product names is for descriptive purposes only and does not imply endorsement by the U.S. Government.

Appendix A. Supplementary data

Supplementary data to this article can be found online at <https://doi.org/10.1016/j.quascirev.2024.108976>.

References

Ager, T.A., 2003. Late Quaternary vegetation and climate history of the central Bering land bridge from St. Michael Island, western Alaska. *Quaternary Research* 60 (1), 19–32. [https://doi.org/10.1016/S0033-5894\(03\)00068-1](https://doi.org/10.1016/S0033-5894(03)00068-1).

Albuhaiisi, Y.A.Y., van der Velde, Y., De Jeu, R., Zhang, Z., Houweling, S., 2023. High-resolution estimation of methane emissions from boreal and pan-Arctic Wetlands using advanced satellite data. *Remote Sens* 15, 3433. <https://doi.org/10.3390/rs15133433>.

Anderson, P.M., 1988. Late quaternary pollen records from the Kobuk and Noatak river drainages, northwestern Alaska. *Quaternary Research* 29 (3), 263–276. [https://doi.org/10.1016/0033-5894\(88\)90035-X](https://doi.org/10.1016/0033-5894(88)90035-X).

Angelopoulos, M., Overduin, P.P., Westermann, S., Tronicke, J., Strauss, J., Schirmeister, L., Biskaborn, B.K., Liebner, S., Maksimov, G., Grigoriev, M.N., Grosse, G., 2020. Thermokarst Lake to lagoon transitions in eastern Siberia: do submerged taliks refreeze? *J. Geophys. Res.: Earth Surf.* 125 (10). <https://doi.org/10.1029/2019JF005424>.

Batchelor, C.L., Margold, M., Krapp, M., Murton, D.K., Dalton, A.S., Gibbard, P.L., Stokes, C.R., Murton, J.B., Manica, A., 2019. The configuration of Northern Hemisphere ice sheets through the Quaternary. *Nat. Commun.* 10 (1), 3713. <https://doi.org/10.1038/s41467-019-11601-2>.

Bauch, H.A., Kassens, H., Naidina, O.D., Kunz-Pirrung, M., Thiede, J., 2001. Composition and flux of Holocene sediments on the eastern Laptev Sea shelf, arctic Siberia. *Quaternary Research* 55 (3), 344–351. <https://doi.org/10.1006/qres.2000.2223>.

Blumenberg, M., Schlömer, S., Reinhardt, L., Scheider, G., Pape, T., Römer, M., 2022. Biomarker insights into a methane-enriched Holocene peat-setting from ‘Doggerland’ (central North Sea). *Holocene* 32 (10), 1015–1025. <https://doi.org/10.1177/09596836221106958>.

Bock, M., Schmitt, J., Beck, J., Seth, B., Chappellaz, J., Fischer, H., 2017. Glacial/interglacial wetland, biomass burning, and geologic methane emissions constrained by dual stable isotopic CH₄ ice core records. *Proc. Natl. Acad. Sci. USA* 114 (29). <https://doi.org/10.1073/pnas.1613883114>.

Bridgman, S.D., Megonigal, J.P., Keller, J.K., Bliss, N.B., Trettin, C., 2006. The carbon balance of North American wetlands. *Wetlands* 26 (4), 889–916. [https://doi.org/10.1672/0277-5212\(2006\)26\[889:TCBONA\]2.0.CO;2](https://doi.org/10.1672/0277-5212(2006)26[889:TCBONA]2.0.CO;2).

Brook, E.J., Harder, S., Severinghaus, J., Steig, E.J., Sucher, C.M., 2000. On the origin and timing of rapid changes in atmospheric methane during the Last Glacial Period. *Global Biogeochem. Cycles* 14 (2), 559–572. <https://doi.org/10.1029/1999GB001182>.

Brook, E.J., Sowers, T., Orchardo, J., 1996. Rapid variations in atmospheric methane concentration during the past 110,000 years. *Science* 273 (5278), 1087–1091. <https://doi.org/10.1126/science.273.5278.1087>.

Brosius, L.S., Anthony, K.M.W., Treat, C.C., Lenz, J., Jones, M.C., Bret-Harte, M.S., Grosse, G., 2021. Spatiotemporal patterns of northern lake formation since the Last Glacial Maximum. *Quat. Sci. Rev.* 253, 106773. <https://doi.org/10.1016/j.quascirev.2020.106773>.

Brosius, L.S., Walter Anthony, K.M., Grosse, G., Chanton, J.P., Farquharson, L.M., Overduin, P.P., Meyer, H., 2012. Using the deuterium isotope composition of permafrost meltwater to constrain thermokarst lake contributions to atmospheric CH₄ during the last deglaciation: δ D constraint of lake CH₄ contributions. *J. Geophys. Res.: Biogeosciences* 117 (G1). <https://doi.org/10.1029/2011JG001810>.

Brosius, L.S., Walter Anthony, K.M., Treat, C.C., Jones, M.C., Dyonisius, M., Grosse, G., 2023. Panarctic lakes exerted a small positive feedback on early Holocene warming due to deglacial release of methane. *Communications Earth & Environment* 4 (1), 271. <https://doi.org/10.1038/s43247-023-00930-2>.

Chang, R.Y.-W., Miller, C.E., Dinardo, S.J., Karion, A., Sweeney, C., Daube, B.C., Henderson, J.M., Mountain, M.E., Eluszkiewicz, J., Miller, J.B., Bruhwiler, L.M.P.,

Wofsy, S.C., 2014. Methane emissions from Alaska in 2012 from CARVE airborne observations. *P. Natl. Acad. Sci.* 111, 16694–16699. <https://doi.org/10.1073/pnas.1412953111>.

Clewley, D., Whitcomb, J., Moghaddam, M., McDonald, K., Chapman, B., Bunting, P., 2015. Evaluation of ALOS PALSAR data for high-resolution mapping of vegetated wetlands in Alaska. *Rem. Sens.* 7 (6), 7272–7297. <https://doi.org/10.3390/rs70607272>.

Corwardin, L.M., Carter, V., Golet, F.C., LaRoe, E.T., 1979. Classification of wetlands and deepwater habitats of the United States. Fish and Wildlife Service, US Department of the Interior.

Danielson, S., Curchitser, E., Hedstrom, K., Weingartner, T., Stabeno, P., 2011. On ocean and sea ice modes of variability in the Bering Sea. *J. Geophys. Res.* 116 (C12), C12034. <https://doi.org/10.1029/2011JC007389>.

Dyke, A.S., Peltier, W.R., 2000. Forms, response times and variability of relative sea-level curves, glaciated North America. *Geomorphology* 32 (3–4), 315–333. [https://doi.org/10.1016/S0169-555X\(99\)00102-6](https://doi.org/10.1016/S0169-555X(99)00102-6).

Dyke, A.S., Savelle, J.M., Johnson, D.S., 2011. Paleoeskimo demography and Holocene seasea-level history, gulf of boothia, arctic Canada. *Arctic* 64 (2), 151–168.

Dyonisius, M.N., Petrenko, V.V., Smith, A.M., Hua, Q., Yang, B., Schmitt, J., Beck, J., Seth, B., Bock, M., Hmiel, B., Vimont, I., Menking, J.A., Shackleton, S.A., Baggenstos, D., Bauska, T.K., Rhodes, R.H., Sperlich, P., Beaudette, R., Harth, C., et al., 2020. Old carbon reservoirs were not important in the deglacial methane budget. *Science* 367 (6480), 907–910. <https://doi.org/10.1126/science.aax0504>.

Edwards, M.E., Anderson, P.M., Brubaker, L.B., Ager, T.A., Andreev, A.A., Bigelow, N.H., Cwynar, L.C., Eisner, W.R., Harrison, S.P., Hu, F.-S., Jolly, D., Lozhkin, A.V., MacDonald, G.M., Mock, C.J., Ritchie, J.C., Sher, A.V., Spear, R.W., Williams, J.W., Yu, G., 2000. Pollen-based biomes for Beringia 18,000, 6000 and 0 14C yr bp +. *J. Biogeogr.* 27 (3), 521–554. <https://doi.org/10.1046/j.1365-2699.2000.00426.x>.

Edwards, M.E., Brubaker, L.B., Lozhkin, A.V., Anderson, P.M., 2005. Structurally novel biomes: a response to past warming in Beringia. *Ecology* 86 (7), 1696–1703. <https://doi.org/10.1890/03-0787>.

Elias, S.A., Short, S.K., Birks, H.H., 1997. Late Wisconsin environments of the bering land bridge. *Palaeogeogr. Palaeoclimatol. Palaeoecol.* 136 (1–4), 293–308. [https://doi.org/10.1016/S0031-0182\(97\)00038-2](https://doi.org/10.1016/S0031-0182(97)00038-2).

Elias, S.A., Short, S.K., Nelson, C.H., Birks, H.H., 1996. Life and times of the Bering land bridge. *Nature* 382 (6586), 60–63. <https://doi.org/10.1038/382060a0>.

Elias, S.A., Short, S.K., Phillips, R.L., 1992. Paleoecology of late-glacial peats from the bering land bridge, Chukchi Sea shelf region, northwestern Alaska. *Quaternary Research* 38 (3), 371–378. [https://doi.org/10.1016/0033-5894\(92\)90045-K](https://doi.org/10.1016/0033-5894(92)90045-K).

Elias, S., Crocker, B., 2008. The Bering Land Bridge: a moisture barrier to the dispersal of steppe-tundra biota? *Quat. Sci. Rev.* 27 (27–28), 2473–2483. <https://doi.org/10.1016/j.quascirev.2008.09.011>.

Engelhart, S.E., Peltier, W.R., Horton, B.P., 2011. Holocene relative sea-level changes and glacial isostatic adjustment of the U.S. Atlantic coast. *Geology* 39 (8), 751–754. <https://doi.org/10.1130/G31857.1>.

England, J.H., Furze, M.F.A., 2008. New evidence from the western Canadian arctic archipelago for the resubmergence of bering strait. *Quaternary Research* 70 (1), 60–67. <https://doi.org/10.1016/j.yqres.2008.03.001>.

Farquharson, L., Anthony, K.W., Bigelow, N., Edwards, M., Grosse, G., 2016. Facies analysis of yedoma thermokarst lakes on the northern Seward Peninsula, Alaska. *Sediment. Geol.* 340, 25–37. <https://doi.org/10.1016/j.sedgeo.2016.01.002>.

Fuchs, M., Jones, M.C., Gowan, E.J., Frolking, S., Walter Anthony, K.M., Grosse, G., Jones, B.M., O'Donnell, J.A., Brosius, L.S., Treat, C.C., 2024a. Data Set for Modeling Methane Fluxes of Beringian Coastal Wetlands, PANGAEA. <https://doi.org/10.1594/PANGAEA.960160>.

Fuchs, M., Jones, M.C., Gowan, E.J., Frolking, S., Walter Anthony, K.M., Grosse, G., Jones, B.M., O'Donnell, J.A., Brosius, L.S., Treat, C.C., 2024b. Methane Flux Measurements from Coastal Wetlands on the Kenai Peninsula, PANGAEA. <https://doi.org/10.1594/PANGAEA.960156>.

Fuchs, M., Jones, M.C., Gowan, E.J., Frolking, S., Walter Anthony, K.M., Grosse, G., Jones, B.M., O'Donnell, J.A., Brosius, L.S., Treat, C.C., 2024c. Modeled Timing of Flooding for the Beringian Shelf for the Past 20,000 Years, PANGAEA. <https://doi.org/10.1594/PANGAEA.960150>.

Gaffney, V., Fitch, S.Hrsg, 2022. Europe's lost frontiers: volume 1. Archaeopress Archaeology. <https://doi.org/10.32028/9781803272689>.

Gavrilov, A.V., Romanovskii, N.N., Romanovsky, V.E., Hubberten, H.-W., Tumskoy, V.E., 2003. Reconstruction of ice complex remnants on the eastern Siberian arctic shelf. *Permaf. Periglac. Process.* 14 (2), 187–198. <https://doi.org/10.1002/ppg.450>.

Gowan, E.J., Zhang, X., Khosravi, S., Rovere, A., Stocchi, P., Hughes, A.L.C., Gyllencreutz, R., Mangerud, J., Svendsen, J.-I., Lohmann, G., 2021. A new global ice sheet reconstruction for the past 80 000 years. *Nat. Commun.* 12 (1), 1199. <https://doi.org/10.1038/s41467-021-21469-w>.

Guthrie, D.R., 2001. Origin and causes of the mammoth steppe: a story of cloud cover, woolly mammal tooth pits, buckles, and inside-out Beringia. *Quat. Sci. Rev.* 20 (1–3), 549–574. [https://doi.org/10.1016/S0277-3791\(00\)00099-8](https://doi.org/10.1016/S0277-3791(00)00099-8).

Hill, P.R., Héquette, A., Ruz, M.-H., 1993. Holocene sea-level history of the Canadian Beaufort shelf. *Can. J. Earth Sci.* 30 (1), 103–108. <https://doi.org/10.1139/e93-009>.

Hill, P.R., Mudie, P.J., Moran, K., Blasco, S.M., 1985. A sea-level curve for the Canadian Beaufort Shelf. *Can. J. Earth Sci.* 22 (10), 1383–1393. <https://doi.org/10.1139/e85-146>.

Hoffecker, J.F., Elias, S.A., Potapova, O., 2020. Arctic Beringia and native American origins. *PaleoAmerica* 6 (2), 158–168. <https://doi.org/10.1080/2055563.2020.1725380>.

Holmquist, J.R., Windham-Myers, L., Bernal, B., Byrd, K.B., Crooks, S., Goncena, M.E., Herold, N., Knox, S.H., Kroeger, K.D., McCombs, J., Megonigal, J.P., Lu, M., Morris, J.T., Sutton-Grier, A.E., Troxler, T.G., Weller, D.E., 2018. Uncertainty in United States coastal wetland greenhouse gas inventory. *Environ. Res. Lett.* 13 (11), 115005. <https://doi.org/10.1088/1748-9326/aae157>.

Hijma, M.P., Cohen, K.M., 2019. Holocene sea-level database for the Rhine-Meuse Delta, The Netherlands: implications for the pre-8.2 ka sea-level jump. *Quat. Sci. Rev.* 214, 68–86. <https://doi.org/10.1016/j.quascirev.2019.05.001>.

Hinkel, K.M., Eisner, W.R., Bockheim, J.G., Nelson, F.E., Peterson, K.M., Dai, X., 2003. Spatial extent, age, and carbon stocks in drained thaw lake basins on the barrow Peninsula, Alaska. *Arctic Antarct. Alpine Res.* 35 (3), 291–300. [https://doi.org/10.1657/1523-0430\(2003\)035\[0291:SEACAJ2.0.CO;2](https://doi.org/10.1657/1523-0430(2003)035[0291:SEACAJ2.0.CO;2).

Hopkins, D.M., 1967. The Bering Land Bridge. Stanford university press.

Jakobsson, M., Mayer, L.A., Bringensparr, C., Castro, C.F., Mohammad, R., Johnson, P., Ketter, T., Accettella, D., Amblas, D., An, L., Arndt, J.E., Canals, M., Casamor, J.L., Chauché, N., Coalkey, B., Danielson, S., Demarte, M., Dickson, M.-L., Dorschel, B., et al., 2020. The international bathymetric chart of the arctic ocean version 4.0. *Sci. Data* 7 (1), 176. <https://doi.org/10.1038/s41597-020-0520-9>.

Jakobsson, M., Pearce, C., Cronin, T.M., Backman, J., Anderson, L.G., Barrientos, N., Björk, G., Coxall, H., de Boer, A., Mayer, L.A., Mörth, C.-M., Nilsson, J., Rattray, J.E., Stranne, C., Semiletov, I., O'Regan, M., 2017. Post-glacial flooding of the Bering Land Bridge dated to 11 cal ka BP based on new geophysical and sediment records. *Clim. Past* 13 (8), 991–1005. <https://doi.org/10.5194/cp-13-991-2017>.

Jenrich, M., Angelopoulos, M., Grosse, G., Overduin, P.P., Schirrmüller, L., Nitze, I., Biskaborn, B.K., Liebner, S., Grigoriev, M., Murray, A., Jongejans, L.L., Strauss, J., 2021. Thermokarst lagoons: a core-based assessment of depositional characteristics and an estimate of carbon pools on the bykovsky Peninsula. *Front. Earth Sci.* 9, 637899. <https://doi.org/10.3389/feart.2021.637899>.

Jones, M.C., Grosse, G., Jones, B.M., Walter Anthony, K., 2012. Peat accumulation in drained thermokarst lake basins in continuous, ice-rich permafrost, northern Seward Peninsula, Alaska. *J. Geophys. Res.* 117, G00M07. <https://doi.org/10.1029/2011JG001766>.

Jongejans, L.L., Strauss, J., 2020. Bootstrapping approach for permafrost organic carbon pool estimation. Zenodo. <https://doi.org/10.5281/ZENODO.3734247> [Software].

Kaplan, J.O., 2002. Wetlands at the last glacial maximum: distribution and methane emissions: wetlands at the last glacial maximum. *Geophys. Res. Lett.* 29 (6). <https://doi.org/10.1029/2001GL013366>, 3–1–3–4.

Kaplan, J.O., Folberth, G., Hauglustaine, D.A., 2006. Role of methane and biogenic volatile organic compound sources in late glacial and Holocene fluctuations of atmospheric methane concentrations: late Glacial and Holocene atmospheric methane. *Global Biogeochem. Cycles* 20 (2). <https://doi.org/10.1029/2005GB002590> n/a–n/a.

Keigwin, L.D., Donnelly, J.P., Cook, M.S., Driscoll, N.W., Brigham-Grette, J., 2006. Rapid sea-level rise and Holocene climate in the Chukchi Sea. *Geology* 34 (10), 861. <https://doi.org/10.1130/G22712.1>.

Kleiber, H.P., Niessen, F., 1999. Late pleistocene paleoriver channels on the Laptev Sea shelf—implications from sub-bottom profiling. In: Kassens, H., Bauch, H.A., Dmitrenko, I.A., Eicken, H., Hubberten, H.-W., Melles, M., Thiede, J., Timokhov (Hrsg. L.A. (Eds.)), *Land-Ocean Systems In the Siberian Arctic* (S. 657–665). Springer Berlin Heidelberg. https://doi.org/10.1007/978-3-642-60134-7_49.

Kleinen, T., Mikolajewicz, U., Brovkin, V., 2020. Terrestrial methane emissions from the Last Glacial Maximum to the preindustrial period. *Clim. Past* 16 (2), 575–595. <https://doi.org/10.5194/cp-16-575-2020>.

Köhler, P., Nehrbass-Ahles, C., Schmitt, J., Stocker, T.F., Fischer, H., 2017. A 156 kyr smoothed history of the atmospheric greenhouse gases CO₂, CH₄, and N₂O and their radiative forcing. *Earth Syst. Sci. Data* 9 (1), 363–387. <https://doi.org/10.5194/essd-9-363-2017>.

Kuhn, M.A., Varner, R.K., Bastviken, D., Crill, P., MacIntyre, S., Turetsky, M., Walter Anthony, K., McGuire, A.D., Olefeldt, D., 2021. BAWLD-CH4: a comprehensive dataset of methane fluxes from boreal and arctic ecosystems. *Earth Syst. Sci. Data* 13, 5151–5189. <https://doi.org/10.5194/essd-13-5151-2021>.

Lenz, J., Wetterich, S., Jones, B.M., Meyer, H., Bobrov, A., Grosse, G., 2016. Evidence of multiple thermokarst lake generations from an 11 800-year-old permafrost core on the northern Seward Peninsula, Alaska. *Boreas* 45, 584–603. <https://doi.org/10.1111/bor.12186>.

Li, T., Khan, N.S., Baranskaya, A.V., Shaw, T.A., Peltier, W.R., Stuhne, G.R., Wu, P., Horton, B.P., 2022. Influence of 3D Earth structure on glacial isostatic adjustment in the Russian arctic. *J. Geophys. Res. Solid Earth* 127 (3). <https://doi.org/10.1029/2021JB023631>.

Liikanen, A., Silvennoinen, H., Karvo, A., Martikainen, P.J., Rantakokko, P., 2009. Methane and nitrous oxide fluxes in two coastal wetlands in the northeastern Gulf of Bothnia. *Boreal Environment Research* 14.

Lippmann, T.J.R., in 't Zandt, M.H., Van der Putten, N.N.L., Busschers, F.S., Hijma, M.P., van der Velden, P., de Groot, T., van Aalderen, Z., Meisel, O.H., Slomp, C.P., Niemann, H., Jetten, M.S.M., Dolman, H.A.J., Welte, C.U., 2021. Microbial activity, methane production, and carbon storage in Early Holocene North Sea peats. *Biogeosciences* 18 (19), 5491–5511. <https://doi.org/10.5194/bg-18-5491-2021>.

MacManus, D.A., Venkataraman, K., Hopkins, D.M., Nelson, H., 1974. Yukon River sediment on the northernmost Bering Sea shelf. *SEPM Journal of Sedimentary Research* 44. <https://doi.org/10.1306/212F6C2B-2B24-11D7-8648000102C1865D>.

Marcott, S.A., Bauska, T.K., Buizert, C., Steig, E.J., Rosen, J.L., Cuffey, K.M., Fudge, T.J., Severinghaus, J.P., Ahn, J., Kalk, M.L., McConnell, J.R., Sowers, T., Taylor, K.C., White, J.W.C., Brook, E.J., 2014. Centennial-scale changes in the global carbon cycle during the last deglaciation. *Nature* 514 (7524), 616–619. <https://doi.org/10.1038/nature13799>.

McGuire, A.D., Genet, H., Lyu, Z., Pastick, N., Stackpoole, S., Birdsey, R., D'Amore, D., He, Y., Rupp, T.S., Striegl, R., Wylie, B.K., Zhou, X., Zhuang, Q., Zhu, Z., 2018. Assessing historical and projected carbon balance of Alaska: a synthesis of results

and policy/management implications. *Ecol. Appl.* 28, 1396–1412. <https://doi.org/10.1002/eaap.1768>.

McLeod, E., Chmura, G.L., Bouillon, S., Salm, R., Björk, M., Duarte, C.M., Lovelock, C.E., Schlesinger, W.H., Silliman, B.R., 2011. A blueprint for blue carbon: toward an improved understanding of the role of vegetated coastal habitats in sequestering CO₂. *Front. Ecol. Environ.* 9 (10), 552–560. <https://doi.org/10.1890/110004>.

McManus, D.A., Creager, J.S., 1984. Sea-Level data for parts of the bering-chukchi shelves of Beringia from 19,000 to 10,000 14C yr B.P. *Quaternary Research* 21 (3), 317–325. [https://doi.org/10.1016/0033-5894\(84\)90071-1](https://doi.org/10.1016/0033-5894(84)90071-1).

Meyer, V.D., Hefter, J., Köhler, P., Tiedemann, R., Gersonde, R., Wacker, L., Mollenhauer, G., 2019. Permafrost-carbon mobilization in Beringia caused by deglacial meltwater runoff, sea-level rise and warming. *Environ. Res. Lett.* 14 (8), 085003. <https://doi.org/10.1088/1748-9326/ab2653>.

Monteath, A.J., Gaglioti, B.V., Edwards, M.E., Froese, D., 2021. Late Pleistocene shrub expansion preceded megafauna turnover and extinctions in eastern Beringia. *Proc. Natl. Acad. Sci. USA* 118 (52), e2107977118. <https://doi.org/10.1073/pnas.2107977118>.

Mueller, P., Mozdzer, T.J., Langley, J.A., Aoki, L.R., Noyce, G.L., Megonigal, J.P., 2020. Plant species determine tidal wetland methane response to sea level rise. *Nat. Commun.* 11 (1), 5154. <https://doi.org/10.1038/s41467-020-18763-4>.

Nelson, H., Creager, J.S., 1977. Displacement of yukon-derived sediment from Bering Sea to Chukchi Sea during Holocene time. *Geology* 5 (3), 141. [https://doi.org/10.1130/091-7613\(1977\)5<141:DOYSFB>2.0.CO;2](https://doi.org/10.1130/091-7613(1977)5<141:DOYSFB>2.0.CO;2).

Olefeldt, D., Hovemyr, M., Kuhn, M., Bastviken, D., Bohn, T.J., Connolly, J., Crill, P., Euskirchen, E.S., Finkelstein, S.A., Genet, H., Grosse, G., Harris, L.I., Heffernan, L., Helbig, M., Hugelius, G., Hutchins, R., Juntinen, S., Lara, M.J., Malhotra, A., Manies, K., McGuire, A.D., Natali, S.M., O'Donnell, J.A., Parmentier, F.-J.W., Räsänen, A., Schädel, C., Sonnentag, O., Strack, M., Tank, S.E., Treat, C., Varner, R.K., Virtanen, T., Warren, R.K., Watts, J.D., 2021. The boreal-arctic wetland and lake dataset (BAWLD). *Earth Syst. Sci. Data* 13, 5127–5149. <https://doi.org/10.5194/essd-13-5127-2021>.

Pastick, N.J., Duffy, P., Genet, H., Rupp, T.S., Wylie, B.K., Johnson, K.D., Jorgenson, M., Bliss, N., McGuire, A.D., Jafarov, E.E., Knight, J.F., 2017. Historical and projected trends in landscape drivers affecting carbon dynamics in Alaska. *Ecol. Appl.* 27, 1383–1402. <https://doi.org/10.1002/eaap.1538>.

Pellerin, A., Lotem, N., Walter Anthony, K., Eliani Russak, E., Hasson, N., Roy, H., Chanton, J.P., Sivan, O., 2022. Methane production controls in a young thermokarst lake formed by abrupt permafrost thaw. *Global Change Biol.* 28 (10), 3206–3221. <https://doi.org/10.1111/gcb.16151>.

Petrenko, V.V., Smith, A.M., Schaefer, H., Riedel, K., Brook, E., Baggenstos, D., Harth, C., Hua, Q., Buijzer, C., Schilt, A., Fain, X., Mitchell, L., Bauska, T., Orsi, A., Weiss, R.F., Severinghaus, J.P., 2017. Minimal geological methane emissions during the Younger Dryas—Preboreal abrupt warming event. *Nature* 548 (7668), 443–446. <https://doi.org/10.1038/nature23316>.

Pico, T., Mitrovica, J.X., Mix, A.C., 2020. Sea level fingerprinting of the Bering Strait flooding history detects the source of the Younger Dryas climate event. *Sci. Adv.* 6 (9), eaay2935. <https://doi.org/10.1126/sciadv.aay2935>.

Poffenbarger, H.J., Needelman, B.A., Megonigal, J.P., 2011. Salinity influence on methane emissions from tidal marshes. *Wetlands* 31 (5), 831–842. <https://doi.org/10.1007/s13157-011-0197-0>.

Ramage, J., Kuhn, M., Virkkala, A.-M., Voigt, C., Marushchak, M.E., Bastos, A., et al., 2024. The net GHG balance and budget of the permafrost region (2000–2020) from ecosystem flux upscaling. *Global Biogeochem. Cycles* 38, e2023GB007953. <https://doi.org/10.1029/2023GB007953>.

Reimer, P.J., Austin, W.E.N., Bard, E., Bayliss, A., Blackwell, P.G., Bronk Ramsey, C., Butzin, M., Cheng, H., Edwards, R.L., Friedrich, M., Grootes, P.M., Guilderson, T.P., Hajdas, I., Heaton, T.J., Hogg, A.G., Hughen, K.A., Kromer, B., Manning, S.W., Muscheler, R., et al., 2020. The IntCal20 northern hemisphere radiocarbon age calibration curve (0–55 cal kBP). *Radiocarbon* 62 (4), 725–757. <https://doi.org/10.1017/RDC.2020.41>.

Reimer, R.W., Reimer, P.J., 2022. CALIBomb [WWW program] [Software]. <http://calib.org>. (Accessed 12 December 2022).

Rinne, J., Tuittila, E.-S., Peltola, O., Li, X., Raivonen, M., Alekseychik, P., et al., 2018. Temporal variation of ecosystem scale methane emission from a boreal fen in relation to temperature, water table position, and carbon dioxide fluxes. *Global Biogeochem. Cycles* 32, 1087–1106. <https://doi.org/10.1029/2017GB005747>.

Rogers, K., Kelleway, J.J., Saintilan, N., Megonigal, J.P., Adams, J.B., Holmquist, J.R., Lu, M., Schile-Beers, L., Zawadzki, A., Mazumder, D., Woodroffe, C.D., 2019. Wetland carbon storage controlled by millennial-scale variation in relative sea-level rise. *Nature* 567 (7746), 91–95. <https://doi.org/10.1038/s41586-019-0951-7>.

Romanovskii, N.N., Hubberten, H.-W., Gavrilov, A.V., Tumskoy, V.E., Tipenko, G.S., Grigoriev, M.N., Siegert, C., 2000. Thermokarst and land-ocean interactions, Laptev sea region, Russia. *Permafrost. Periglac. Process.* 11 (2), 137–152. [https://doi.org/10.1002/1099-1530\(200004/06\)11:2<137::AID-PPP345>3.0.CO;2-L](https://doi.org/10.1002/1099-1530(200004/06)11:2<137::AID-PPP345>3.0.CO;2-L).

Rosentreter, J.A., Borges, A.V., Deemer, B.R., Holgerson, M.A., Liu, S., Song, C., Melack, J., Raymond, P.A., Duarte, C.M., Allen, G.H., Olefeldt, D., Poulter, B., Battin, T.I., Eyre, B.D., 2021a. Half of global methane emissions come from highly variable aquatic ecosystem sources. *Nat. Geosci.* 14 (4), 225–230. <https://doi.org/10.1038/s41561-021-00715-2>.

Rosentreter, J.A., Al-Haj, A.N., Fulweiler, R.W., Williamson, P., 2021b. Methane and nitrous oxide emissions complicate coastal blue carbon assessments. *Global Biogeochem. Cycles* 35 (2). <https://doi.org/10.1029/2020GB006858>.

Rosentreter, J.A., Maher, D.T., Erler, D.V., Murray, R.H., Eyre, B.D., 2018. Methane emissions partially offset “blue carbon” burial in mangroves. *Sci. Adv.* 4 (6), eaao4985. <https://doi.org/10.1126/sciadv.aao4985>.

Roth, F., Sun, X., Geibel, M.C., Prytherch, J., Brücher, V., Bonaglia, S., Broman, E., Nascimento, F., Norkko, A., Humborg, C., 2022. High spatiotemporal variability of methane concentrations challenges estimates of emissions across vegetated coastal ecosystems. *Global Change Biol.* 28, 4308–4322. <https://doi.org/10.1111/gcb.16177>.

Saunois, M., Stavert, A.R., Poulter, B., Bousquet, P., Canadell, J.G., Jackson, R.B., Raymond, P.A., Dlugokencky, E.J., Houweling, S., Patra, P.K., Ciais, P., Arora, V.K., Bastviken, D., Bergamaschi, P., Blake, D.R., Braeisford, G., Bruhwiler, L., Carlson, K.M., Carroll, M., Castaldi, S., Chandra, N., Crevoisier, C., Crill, P.M., Covey, K., Curry, C.L., Etiopic, G., Frankenberger, C., Gedney, N., Hegglin, M.I., Höglund-Isaksson, L., Hugelius, G., Ishizawa, M., Ito, A., Janssens-Maenhout, G., Jensen, K.M., Joos, F., Kleinen, T., Krummel, P.B., Langenfelds, R.L., Laruelle, G.G., Liu, L., Machida, T., Maksyutov, S., McDonald, K.C., McNorton, J., Miller, P.A., Melton, J.R., Morino, I., Müller, J., Murguia-Flores, F., Naik, V., Niwa, Y., Noce, S., O'Doherty, S., Parker, R.J., Peng, C., Peng, S., Peters, G.P., Prigent, C., Prinn, R., Ramonet, M., Regnier, P., Riley, W.J., Rosentreter, J.A., Segers, A., Simpson, J.D., Shi, H., Smith, S.J., Steele, L.P., Thornton, B.F., Tian, H., Tohjima, Y., Tubiello, F.N., Tsuruta, A., Viovy, N., Voulgarakis, A., Weber, T.S., van Weele, M., van der Werf, G.R., Weiss, R.F., Worthy, D., Wunch, D., Yin, Y., Yoshida, Y., Zhang, W., Zhang, Z., Zhao, Y., Zheng, B., Zhu, Q., Zhu, Q., Zhuang, Q., 2020. The global methane budget 2000–2017. *Earth Syst. Sci. Data* 12, 1561–1623. <https://doi.org/10.5194/essd-12-1561-2020>.

Schirrmeister, L., Froese, D., Tumskoy, V., Grosse, G., Wetterich, S., 2013. Yedoma: late pleistocene ice-rich syngenetic permafrost of Beringia. In: *Encyclopedia of Quaternary Science*. 2nd Edition. Elsevier, Amsterdam, pp. 542–552.

Severinghaus, J.P., Brook, E.J., 1999. Abrupt climate change at the end of the last glacial period inferred from trapped air in polar ice. *Science* 286 (5441), 930–934. <https://doi.org/10.1126/science.286.5441.930>.

Shakhova, N., Semiletov, I., Chuvilin, E., 2019. Understanding the permafrost–hydrate system and associated methane releases in the East Siberian arctic shelf. *Geosciences* 9 (6), 251. <https://doi.org/10.3390/geosciences9060251>.

Shennan, I., 1982. Interpretation of flandrian sea-level data from the fenland, England. *PGA (Proc. Geol. Assoc.)* 93 (1), 53–63. [https://doi.org/10.1016/S0016-7878\(82\)80032-1](https://doi.org/10.1016/S0016-7878(82)80032-1).

Sher, A.V., 1991. A brief overview of the late-cenozoic history of the western beringian lowlands. In: *Terrestrial Paleoenvironmental Studies in Beringia* (S. 3–6).

Shurpali, N.J., Verma, S.B., Clement, R.J., Billesbach, D.P., 1993. Seasonal distribution of methane flux in a Minnesota peatland measured by eddy correlation. *J. Geophys. Res.* 98 (D11), 20649–20655. <https://doi.org/10.1029/93JD02181>.

Solomon, S., Mudie, P.J., Cranston, R., Hamilton, T., Thibaudeau, S.A., Collins, E.S., 2000. Characterisation of marine and lacustrine sediments in a drowned thermokarst embayment, Richards Island, Beaufort Sea, Canada. *Int. J. Earth Sci.* 89 (3), 503–521. <https://doi.org/10.1007/s005310000126>.

Stolbovoi, V., McCallum, I., 2002. Land resources of Russia [CD-ROM]. Laxenburg, Austria. International Institute for Applied Systems Analysis and the Russian Academy of Science.

Strauss, J., Laboor, S., Schirrmeister, L., Fedorov, A.N., Fortier, D., Froese, D., Fuchs, M., Günther, F., Grigoriev, M., Harden, J., Hugelius, G., Jongejans, L.L., Kanevskiy, M., Kholodov, A., Kunitsky, V., Kraev, G., Lozhkin, A., Rivkina, E., Shur, Y., et al., 2021. Circum-arctic map of the yedoma permafrost domain. *Front. Earth Sci.* 9, 758360. <https://doi.org/10.3389/feart.2021.758360>.

Strauss, J., Schirrmeister, L., Grosse, G., Fortier, D., Hugelius, G., Knoblauch, C., Romanovsky, V., Schädel, C., Schneider von Deimling, T., Schuur, E.A.G., Shmelenov, D., Ulrich, M., Veremeeva, A., 2017. Deep Yedoma permafrost: a synthesis of depositional characteristics and carbon vulnerability. *Earth Sci. Rev.* 172, 75–86. <https://doi.org/10.1016/j.earscirev.2017.07.007>.

Taylor, J., 1997. *Introduction to Error Analysis, the Study of Uncertainties in Physical Measurements*, vol. 2. University science books, Mill Valley, CA, pp. 193–200.

Törnqvist, T.E., van Ree, M.H.M., van 't Veer, R., van Geel, B., 1998. Improving methodology for high-resolution reconstruction of sea-level rise and neotectonics by paleoecological analysis and AMS 14C dating of basal peats. *Quaternary Research* 49 (1), 72–85. <https://doi.org/10.1006/qres.1997.1938>.

Treat, C.C., Bloom, A.A., Marushchak, M.E., 2018. Nongrowing season methane emissions—a significant component of annual emissions across northern ecosystems. *Global Change Biol.* 24 (8), 3331–3343. <https://doi.org/10.1111/gcb.14137>.

Treat, C.C., Jones, M.C., Brosius, L., Grosse, G., Walter Anthony, K., Frolking, S., 2021. The role of wetland expansion and successional processes in methane emissions from northern wetlands during the Holocene. *Quat. Sci. Rev.* 257, 106864. <https://doi.org/10.1016/j.quascirev.2021.106864>.

Treat, C.C., Virkkala, A.-M., Burke, E., Bruhwiler, L., Chatterjee, A., Fisher, J.B., et al., 2024. Permafrost carbon: progress on understanding stocks and fluxes across northern terrestrial ecosystems. *J. Geophys. Res.: Biogeosciences* 129, e2023JG007638. <https://doi.org/10.1029/2023JG007638>.

Turner, J.N., Macklin, M.G., Jones, A.F., Lewis, H., 2010. New perspectives on Holocene flooding in Ireland using meta-analysis of fluvial radiocarbon dates. *Catena* 82 (3), 183–190. <https://doi.org/10.1016/j.catena.2010.06.004>.

UNFCCC, & IUCN, 2022. Innovative approaches for strengthening coastal and ocean adaptation—integrating technology and nature-based solutions. United Nations Climate Change Secretariat 25. ISBN: 978-92-9219-202-0. <https://unfccc.int/sites/default/files/resource/InnovativeApproachesforStrengtheningCoastaland%20Oceans.pdf>.

Valdes, P.J., Beerling, D.J., Johnson, C.E., 2005. The ice age methane budget. *Geophys. Res. Lett.* 32 (2), L02704. <https://doi.org/10.1029/2004GL021004>.

Winterfeld, M., Mollenhauer, G., Dummann, W., Köhler, P., Lembke-Jene, L., Meyer, V., Hefter, J., McIntyre, C., Wacker, L., Kokfelt, U., Tiedemann, R., 2018. Deglacial mobilization of pre-aged terrestrial carbon from degrading permafrost. *Nat. Commun.* 9 (1), 3666. <https://doi.org/10.1038/s41467-018-06080-w>.

Wolters, S., Zeiler, M., Bungenstock, F., 2010. Early Holocene environmental history of sunken landscapes: pollen, plant macrofossil and geochemical analyses from the Borkum Riffgrund, southern North Sea. *Int. J. Earth Sci.* 99 (8), 1707–1719. <https://doi.org/10.1007/s00531-009-0477-6>.

Wong, P.P., Losada, I.J., Gattuso, J.-P., Hinkel, J., Khattabi, A., McInnes, K.L., Saito, Y., Sallenger, A., 2014. Coastal systems and low-lying areas. In: *Climate Change 2014: Impacts, Adaptation and Vulnerability. Part A: Global and Sectoral Aspects*. Contribution of Working Group II to the Fifth Assessment Report of the Intergovernmental Panel on Climate Change (S. 361–409). Cambridge University Press.

Yamazaki, D., Ikeshima, D., Tawatari, R., Yamaguchi, T., O'Loughlin, F., Neal, J.C., Sampson, C.C., Kanae, S., Bates, P.D., 2017. A high-accuracy map of global terrain elevations: accurate Global Terrain Elevation map. *Geophys. Res. Lett.* 44 (11), 5844–5853. <https://doi.org/10.1002/2017GL072874>.

Yang, J.-W., Ahn, J., Brook, E.J., Ryu, Y., 2017. Atmospheric methane control mechanisms during the early Holocene. *Clim. Past* 13 (9), 1227–1242. <https://doi.org/10.5194/cp-13-1227-2017>.

Yurtsev, B.A., 2001. The Pleistocene “Tundra-Steppe” and the productivity paradox: the landscape approach. *Quat. Sci. Rev.* 20 (1–3), 165–174. [https://doi.org/10.1016/S0277-3791\(00\)00125-6](https://doi.org/10.1016/S0277-3791(00)00125-6).